

Miljø og samfunnstjenlige tunneler

Prediction of leakage into Lunner tunnel based on discrete fracture flow models

20001042-2

4 March 2003

I henhold til NGIs kvalitetssikringssystem, kan NGI kun bli holdt ansvarlig for den signerte versjonen av denne rapporten. Denne kan på anmodning ettersendes med ordinær post.

Rapporten må ikke benyttes i utdrag eller til andre formål enn det rapporten omhandler. Den må ikke leveres til tredjemann uten oppdragsgivers samtykke. Rapporten må ikke reproduseres.

In accordance with NGIs quality assurance system, NGI can only be held responsible for the signed version of this report. On request, this can be sent by ordinary mail.

This report shall not be used in parts, nor for other purposes than the report deals with. The report shall not be given to a third party without the proprietor's (client's) consent. This report shall not be copied, in parts or in whole.



rapport/report

Miljø og samfunnstjenlige tunneler

Prediction of leakage into Lunner tunnel based on discrete fracture flow models

20001042-2

4 March 2003

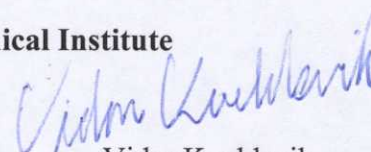
Client: **Prosjektet Miljø- og
Samfunnstjenelige tunneler**

Contact person: Alf Trygve Kveen, Statens
vegvesen, Vegteknisk kontor


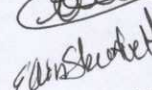
Contract reference: Letter dated 2/3/2001

For the Norwegian Geotechnical Institute

Project Manager:


Vidar Kveldsvik

Report prepared by:


Fabrice Cuisiat

Elin Skurtveit

Reviewed by:

Vidar Kveldsvik

Work also carried out by:

Finn Løvholt

Summary

As part of the project “Tunnels for the citizen”, sub-project B “Environmental concerns”, coordinated by the Norwegian Road Authority (“Statens vegvesen”), a discrete fracture network model was used to investigate the hydrogeological conditions before and after construction of the Lunner tunnel.

A limited model was considered which covers an area of 550 m x 550 m comprising the transition zone from two rock types (hornfels and syenite) where potential problems were foreseen. Available data from site investigation performed by Statens vegvesen and NGU was used to build the model. First, large scale features which could be geologically mapped were represented deterministically. Smaller scale features which could only be characterised in a statistical sense from boreholes observation in terms of orientation, dip, length, density were used to stochastically generate discrete fracture networks through which water flows. Saturated transient and steady state calculations were performed to predict the amount of leakage into the tunnel during construction. Only linear groundwater flow was considered, with a constant recharge from precipitation. Due to the uncertainty related to crucial input parameters such as fracture length and fracture hydraulic properties, a parametric analysis was carried out to investigate the range of variation in the model predictions.

The results from the modelling give a three dimensional picture of the groundwater level after tunnel excavation. They outline the interrelation between tunnel and main conductive faults in the establishment of a lowered water table. Due to tunnel excavation, a rapid drawdown is established above the tunnel and propagates into the rock mass along conductive fault zones. Injection of the faulted zone contributes to a drastic reduction in leakage rates in the whole tunnel, although locally the water inflow increased on both sides of the injection interval through secondary fracture sets.

The work presented in this report contributed to:

- assess the capabilities of discrete fracture network models generally, and more specifically their application to modelling of groundwater flow around tunnels in fractured rock masses
- test the commercial software Napsac used for the purpose of the analyses
- carry out a blind prediction of the effect associated with tunnel excavation in a potentially sensitive area, based on data collected during pre-investigation work
- evaluate the results from discrete fracture modelling and the sensitivity to input parameters. Of particular interest were the correlations between tunnel leakage, pore pressure changes and groundwater drawdown, which could be used to define acceptance criteria for tunnel leakage based on the vulnerability of vegetation and water sources.



Contents

1	INTRODUCTION.....	5
1.1	The project.....	5
1.2	The modelling tool, NAPSAC.....	5
1.3	Basic assumptions underlying the stochastic network approach.....	6
2	SITE DESCRIPTION AND DATA COLLECTION	8
2.1	The geology of the area	8
2.2	The area of interest	8
2.3	Data collection for discrete fracture modelling	9
2.3.1	Identification of major faults and fracture zones.....	12
2.3.2	Definition of fracture sets and orientation.....	12
2.3.3	Estimation of fracture frequencies.....	14
2.3.4	Estimation of fracture shape and size.....	16
2.3.5	Fracture distribution in space	17
2.3.6	Summary of geometrical input parameters.....	17
2.4	Estimation of hydraulic properties of fractures	18
2.4.1	Observation from Lugeon tests performed in Statens vegvesen borehole 1	18
2.4.2	Observation from NGU boreholes.....	20
2.4.3	Distribution of transmissivities.....	20
2.4.4	Fracture storativity.....	20
2.5	Hydraulic calibration of fracture networks.....	22
2.6	In situ and boundary hydrogeological conditions for the site.....	26
3	PREDICTION OF TUNNEL INFLOWS FROM FRACTURE NETWORK MODELLING	26
3.1	Introduction.....	26
3.2	Estimation of model size and characteristic time scales involved in transient flow.....	27
3.2.1	Effect of model size.....	27
3.2.2	Characteristic times involved in unsaturated flow	29
3.3	The Napsac numerical model	31
3.3.1	The modelling region.....	31
3.3.2	The tunnel	32
3.3.3	Initial and boundary conditions	32
3.4	Sensitivity analysis	33
3.4.1	Effect of background fractures (stochastic).....	33
3.4.2	Effect of faults – fracture zones (deterministic).....	34
3.4.3	Effect of transmissivity distribution	36
3.4.4	Effect of boundary conditions and permeability contrast.....	37
3.4.5	Discussion of the results	43
3.5	The effect of cement injection	45
3.5.1	Introduction	45
3.5.2	Result of cement injection along the whole tunnel.....	46



3.5.3	Result of cement injection within an interval.....	48
4	CONCLUSIONS AND RECOMMENDATIONS FOR FUTURE WORK	51
4.1	Conclusions.....	51
4.2	Recommendations for future work	53
5	REFERENCES.....	55

Review and reference document



1 INTRODUCTION

As part of the project “Tunnels for the citizen”, sub-project B “Environmental concerns”, coordinated by the Norwegian Road Authority (Statens vegvesen), a 3D hydrogeological model of an area next to Langvatnet, Lunner has been built to evaluate the consequence of a tunnel excavation on the environment, especially groundwater conditions (lowering of the water table), and predict water inflow into the tunnel during excavation and cement injection.

The model is based on a three-dimensional representation of the conductive fracture network in a rock mass, which was built from available data collected during site investigations and borehole testing as well as open literature. Transient and steady state flow through the discrete fracture network are solved by a finite element technique using a commercial software called Napsac. To the author’s knowledge, the method has not been used previously in Norway during site pre-investigations and planning of tunnel projects. One objective of the study was therefore to assess the benefit of such method for impact assessment of tunnels on the environment.

This report describes in details data collection and results from numerical simulations of tunnel excavation and cement injection in fractured zones.

1.1 The project

In order to facilitate the road traffic between Hadeland, Tyrilfjorden, Randsfjorden and the new main airport in Gardemoen, a new road junction between Rv 4 in the west and Rv 174 in the east is under construction. The junction length is 26 km long, including a 3.8 km long tunnel between Gualia and Brovoll in the western part under the Dalasjøhøgda, Langvatnet and the nature reserve of Rinilhaugen. In this section, wetland areas can be very sensitive to lowering of the groundwater table which may be caused by water leakage into the tunnel. In Sub-project B “Environmental concerns”, correlations between tunnel leakage, pore pressure changes and damage to the environment have been investigated by NGI, Norconsult, Jordforsk and NINA to provide classifications of acceptance criteria for tunnel leakage and vulnerability of vegetation and water sources. More information on the project can be found from the project webpage www.tunneler.no.

1.2 The modelling tool, NAPSAC

The Napsac computer program has been developed by AEA Technology throughout the past 10 years for modelling specifically groundwater flow and transport in fractured rock. The program has been extensively verified and results from validation exercises in particular for the Stripa project have also been published (Herbert et al., 1992). In solid rock, where the matrix permeability is low, the main flow occurs in connected networks of fractures.

This provides a very heterogeneous system that may be modelled using a discrete fracture network approach where the individual fractures are described. The fracture networks in the model are generated using a stochastic approach based on fracture sets characterised by statistical description of the input parameters. Also known fractures or zones of weakness are implemented into the model, as well as tunnels and wells. A fine discretisation of the fracture surfaces is used to model accurately fracture intersection and flow. The numerical solution is based on the finite element method which uses an efficient numerical technique on each individual fracture.

For a full description of Napsac, the reader is referred to Wilcock (1996), Hartley (1998). The main assumptions underlying the discrete fracture network approach are recalled in the next section. Note that in Napsac, the pressure variable is the dynamic pressure P_{res} (referred to as residual pressure in Napsac's manual), which is given in terms of the total pressure P as:

$$P_{res} = P + \rho g z \quad (1.1)$$

where ρ is the density of the groundwater, g the acceleration due to gravity and z is the vertical height relative to some datum. P_{res} will be subsequently referred to as the pressure in the Napsac plot outputs.

1.3 Basic assumptions underlying the stochastic network approach

In the approach adopted in the current study, the hydrogeological properties of the fractured rock mass are found by computing the flow characteristics of a three-dimensional stochastic network of finite planes, under the following assumptions:

- the rock matrix is impermeable, such that flow occurs in the fractures only
- individual fractures are represented as rectangular two-dimensional finite planes
- flow within a fracture is represented by two dimensional linear flow. This involves solving for the flux per unit area integrated across the fracture, q :

$$\mathbf{q} = -T \nabla h \quad (1.2)$$

where ∇ is the differential operator $\nabla = \frac{\partial}{\partial x} i + \frac{\partial}{\partial y} j + \frac{\partial}{\partial z} k$, h is the head and T is the fracture transmissivity, given by:

$$T = \frac{\rho g}{12\mu} e^3 \quad (1.3)$$

where ρ and μ are the density and viscosity of the fluid, g is the acceleration due to gravity, and e is the hydraulic aperture of the fracture. Note that the aperture can be non-uniformly distributed onto the discretised fracture plane, in order to simulate effects such as channelling, in which the fluid flow is restricted to channels pathways) within the fracture.

- The physical fracture network is modelled by generating networks of planes whose geometrical characteristics (positions, lengths, orientations) are statistically the same as determined in the field.
- Flow through the fracture network is represented by the flow solution for the stochastic network of two-dimensional planes, with the flow in individual fractures given by Eq. (1.2). The overall solution is found by assuming mass conservation for each plane:

$$\nabla \cdot \mathbf{q} = 0 \quad (1.4)$$

As noted above the network is stochastically generated from statistical fracture data determined from the field. Hence a large amount of fracture geometry data available from boreholes can be used. These data are difficult to use in a deterministic approach, because usually only the major fractures can be correlated between boreholes. However, the resulting network is only statistically equivalent to the unknown field network, and an ensemble of stochastic networks (realisations) should be generated in order to assess the mean flow behaviour and error bounds of the solution.

However, as noted by Dershowitz (1993), the intensity of geological or mapped fractures, P_{32g} is generally much higher than the intensity of conductive fracture intensity P_{32c} , i.e. the intensity of fractures which are capable of carrying significant groundwater flows. In both cases, the intensities are specified as fracture surface area per unit volume (unit in m^{-1}). In a series of applications in Europe, Japan and North America, P_{32c} has been found to be approximately 1 to 15% of P_{32g} for large scale flow problems (see section 2.3.3 for more discussion on P_{32}).

In the present study, in order to limit the computational effort, the stochastic fracture network generated refers to the network of conductive fractures present in the rock mass. Consequently, the network represents only a fraction of the geological network as observed from trace maps or borehole fracture logging.

2 SITE DESCRIPTION AND DATA COLLECTION

2.1 The geology of the area

The bedrock in Gualia belongs to the Oslo field, an area with great geologic activity like faulting, volcanism and intrusions of magma during Carboniferous-Permian time. The bedrock around the planned tunnel was originally dark grey schist with layers of limestone and sandstone. In the eastern part of the area there is a volcanic rock, mainly lava and some conglomerate. An intrusion of syenite in Permian time caused a contact metamorphoses of the schist and it is now found as a hard fine-grained hornfels. The contact with the lava is also intrusive.

The hornfels-syenite contact is found to be a major zone of weakness, with increased fracturing. Several other zones of weakness were identified with geophysical methods and these sites were chosen for drilling of wells and test pumping.

2.2 The area of interest

A 550 m x 550 m area west of Langvatnet has been selected for the flow modelling (Fig 2.1 and Fig 2.2). This is the area with the N-S striking contact between the hornfels and syenite. The western side of the model is a topographical height and there is a 0.25 gradient down to the Langvatnet on the eastern side of the model. The tunnel trace is approximately in an east-west direction through the area of interest.

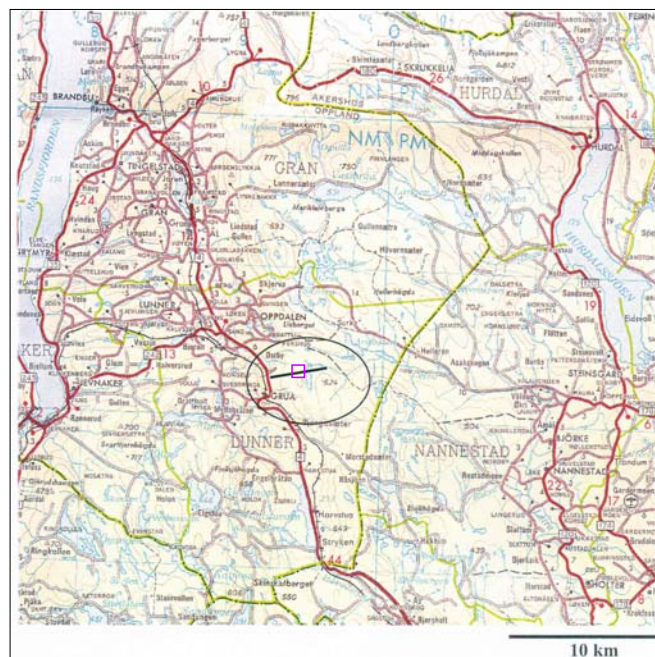


Fig. 2.1 Location map of tunnel trace (black line) and the model area (purple square) next to the Langvatnet in Lunner kommune.

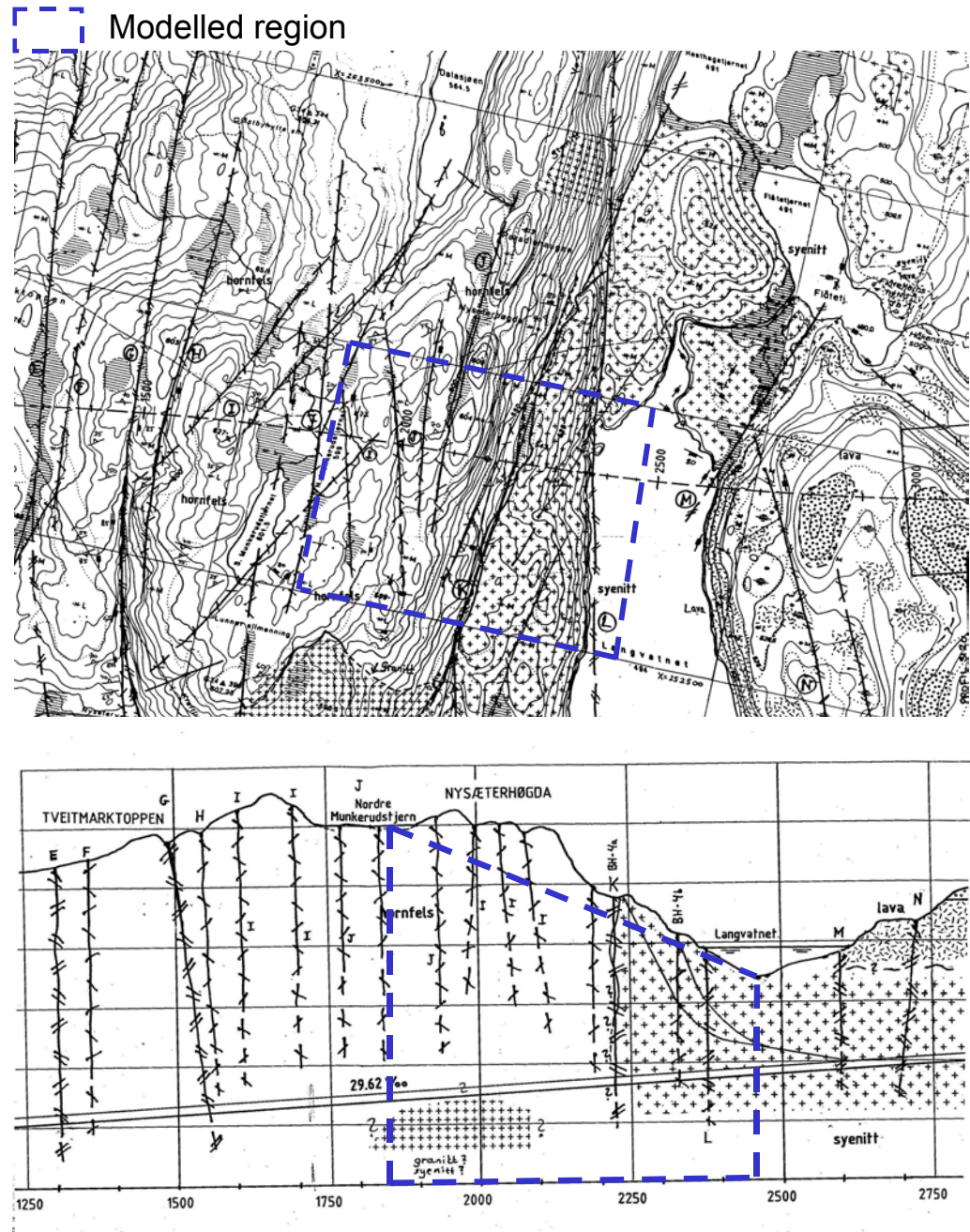


Fig. 2.2 Plan view (top) and cross-section (bottom) of model region. Main structural features and tunnel location are indicated on the map (from Kirkeby & Iversen, 1996)

2.3 Data collection for discrete fracture modelling

In connection with tunnel construction several site investigations have been performed over the last 7 years. A review is given by Holmøy (2002) and summarised in Table 2.1. Geological pre-investigations are described by Kirkeby & Iversen (1996) and core logging are described by Iversen (1998). Different geophysical methods have been tested by NGU in order to

characterise rock mass heterogeneity (Beard 2001, Rønning & Dalsegg 2001). Geological field work and borehole logging with televiewer have also been carried out (Elvebakk et al 2001). Pump tests have been carried out in boreholes (Storrø & Elvebakk, 2002). The hydrological consequence of the tunnel on the surroundings is assessed by Kløve et al. (1999) and an estimation of tunnel leakage is made by Holmøy (2002) based on a synthesis of all data.

Table 2.1 Site investigations in connection with construction of Lunner tunnel

Type of investigation	Date of execution	Type of data collected	Reference
Field mapping	Sept - Oct 1994 and July - Sept 1995	geological description, fault zones	Kirkeby, Iversen, Statens Vegvesen, Oppdarg E-218, Rapport No2 (1996)
Refraction seismic over Langevatn	1997	seismic velocity profiles	Geomap report 97.943 nr 1 (1997)
Core Drilling under Langevatn	Oct.1997 - Jan.1998	Rock mass quality and leakage potential under Langevatn	Statens Vegvesen Oppdrag E218 Rapport No3 (1998)
Aerial measurements - Geophysics anomalies	June 1997 & July 2000	Magnetic, radiometric, electromagnetic and VLF data	NGU Rapport 2001.046 - Miljø og Samfunnstjenlige Tunneler Rapport No 5 (2001)
Ground geophysics & borehole logging	June / July 2001	2D resistivity measurements, Very Low Frequency measurements, magnetometry resistivity	NGU Rapport 2001.090 - Miljø og Samfunnstjenlige Tunneler Rapport No 7 (2001)
Borehole logging & structure geology mapping	Nov. 2001	Optical televiewer, temperature, thermal conductivity, Gamma log	NGU Rapport 2001.117 - Miljø og Samfunnstjenlige Tunneler Rapport No 10 (2001)

The data required for modelling flow through a discrete fracture network concern specifically:

- the geometrical characteristics of the fracture network
 - the definition of large deterministic fractures / fault zones

- the identification of independent fracture sets and the distribution of orientation
- the fracture location in space and the fracture density
- the distribution of fracture length / width
- the hydraulic characteristics of the fracture network
- the distribution of fracture transmissivities (or equivalent hydraulic apertures).

Although the objectives of the site investigation were to characterise the geometrical and hydraulic properties of the fracture network, a complete set of input data required by the discrete fracture model could not be defined due to the following:

- Most wells were vertically drilled, hence intersecting fewer of the dominant vertical fractures.
- As shown in Fig. 2.3, most of the boreholes drilled during site investigation were rather shallow, except for Statens vegvesen borehole 1, which was drilled down to anticipated tunnel level. Hence it is probable that the characteristics of the fracture network as inferred from the exploration boreholes are not fully representative of the whole fracture network especially at depth.

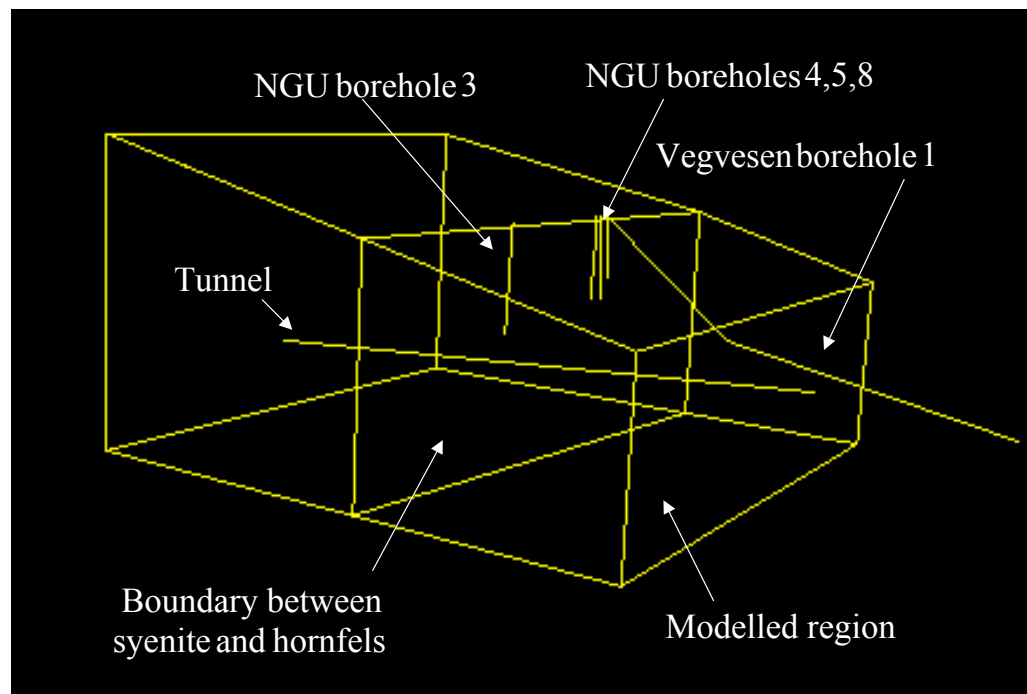


Fig. 2.3 Sketch depicting the volume of interest (for modelling purposes) together with the extent of exploration boreholes available during site investigation. Most of the boreholes characterise only the upper part of the volume of interest.

- Hydraulic packer tests were not performed in testing intervals. These tests could have provided a better characterisation of the hydraulic properties of individual fractures / fault zones.
- Due to difficult ground access, an estimate of fracture / fault length from site investigation was not possible. Fracture mapping from the tunnel surface was not provided, as the aim of the project was to carry out predictions in the pre-investigation phase of tunnel design.

In the following, an attempt is made to define the key parameters used to characterise a fracture network from available field data.

2.3.1 Identification of major faults and fracture zones

Major vertical fracture zones / faults identified from fieldwork and geophysical measurements are included deterministically in the model. In the region of interest, the most important N-S structure follows the contact between hornfels and syenite (zone K). The zone is circa 20 m thick, and shows intense fracturing in tension and shear (slickensides). The zone has been characterised as shear zone, with typical fracture frequency in the order of 3-10 fractures /m in the distal part (Elvebakk et.al. 2002). Other structures have been mapped as shown in Fig.2.2. There is some uncertainty regarding their extent with depth.

2.3.2 Definition of fracture sets and orientation

Geological field investigations (Kirkeby & Iversen, 1996, Elvebakk et al, 2002) shows two dominating fracture trends, N-S and WNW-ESE, and other minor trends in the area which are not implemented into the model (Fig. 2.4).

The televiwer logs carried out in NGU boreholes 3,4,5 and 8 show that half of the fractures identified have a N-S orientation +/- 15° (Fig. 2.5). Also some W to WNW trending fractures are observed and a large number of sub-horizontal fractures, especially in boreholes 3 and 4.

Modelled region

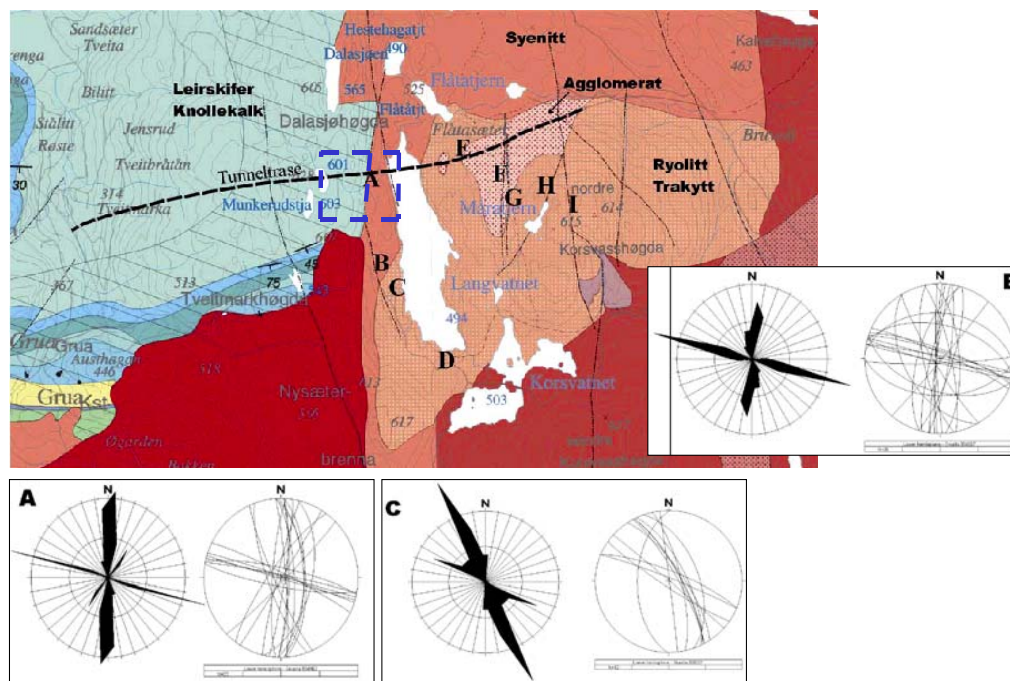


Fig. 2.4 Fracture rose diagrams from site investigation at closest locations from modelled region (data from Elvebakk et al., 2002).

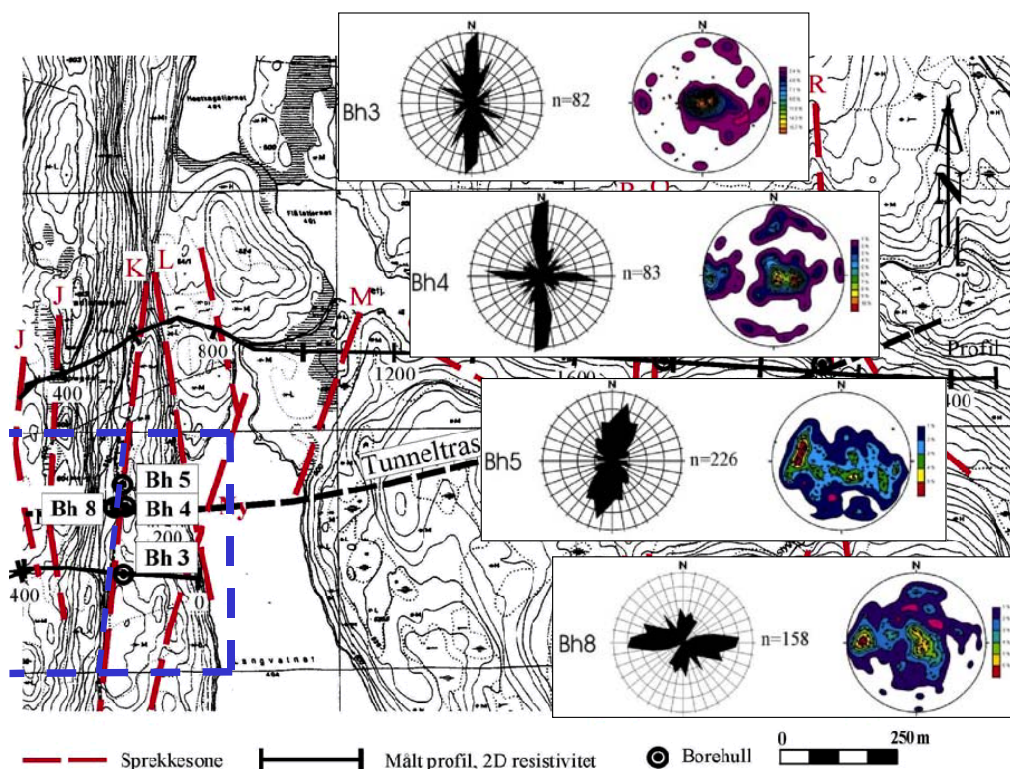


Fig. 2.5 Fracture rose diagrams from NGU boreholes within modelled region (data from Elvebakk et al., 2002).

Stereographic projections of the fractures detected with an optical televiewer (water conductive and not conductive) are shown in Fig. 2.6. Distinct groups have been defined by NGU on the basis of fracture dip and strike.

Based on the previous observations, 2 dominant sub-vertical fracture sets are defined in the discrete fracture model: N-S and WNW-ESE with a 75° to 90° dip, towards the east or west. In addition a sub-horizontal fracture set is defined. In the absence of data pertaining to the hornfels rock type, the same fracture sets have been assumed for both rock formations (hornfels and syenite). Based on experience it is anticipated that the hornfels are more fractured than the syenite, although the fractures can be tighter and less water conductive.

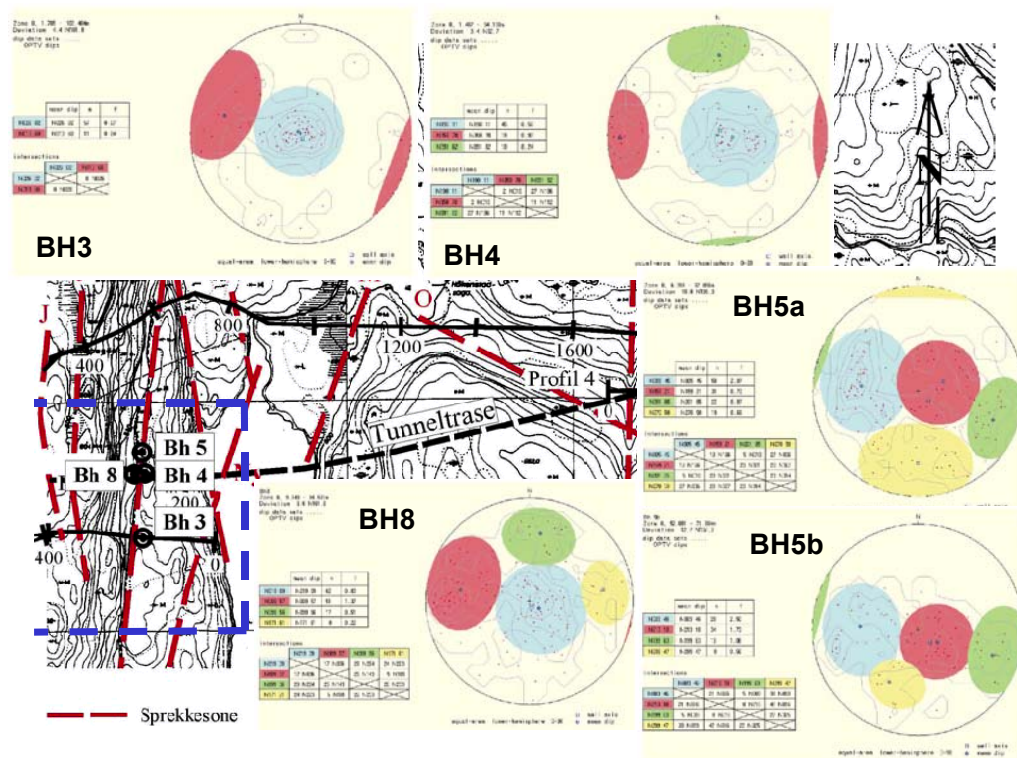


Fig. 2.6 Stereographic projections of fractures detected from NGU boreholes (from Elvebakk et al., 2002).

2.3.3 Estimation of fracture frequencies

Fracture frequency reported in NGU or Statens vegvesen reports refers to geological fracture frequency λ . Several quantities are proposed in the literature to characterise fracture frequency. Strictly speaking, since the fracture frequency ought to be independent from the fracture orientation and volume of interest, the intensity of fractures P_{32} is usually used for statistical modelling purposes. The relationship between λ (referred to as P_{10}) and P_{32} is illustrated in Fig.2.7.

		Dimension of feature				
		0	1	2	3	
Dimension of sampling region	0	P00 (.) Number of fractures samples per point samples of rock mass				Point measures
	1	P10 (m⁻¹) Number of fractures per unit length of scanline (frequency)	P11 (.) Length of fracture intersects per unit length of scanline			Linear measures
	2	P20 (m⁻²) Number of trace centers per unit area of sampling surface (aerial density)	P21 (m⁻¹) Length of fracture traces per unit area of sampled surface (Trace intensity)	P22 (.) Area of fractures per unit area of sampling planes (areal porosity)		Areal measures
	3	P30 (m⁻³) Number of fracture centers per unit volume of rock mass (volumetric density)		P32 (m⁻¹) Area of fractures per unit volume of rock mass (volumetric intensity)	P33 (.) Volume of fractures per unit volume of rock (fracture porosity)	Volumetric measures
		Density		Intensity	Porosity	

etter Golder Associates (2001)

Fig. 2.7 Different quantities used to characterise fracture frequency.

As mentioned in the introduction, the intensity of geological or mapped fractures (expressed as fracture surface per volume of rock), P_{32g} is generally much higher than the intensity of conductive fracture P_{32c} , i.e. the intensity of fractures which are capable of carrying significant groundwater flows. The ratio between P_{32c} and P_{32g} varies between 1 to 15%. In the discrete fracture flow model, only the conductive fractures are considered, so that the fracture intensity is much lower than that observed from borehole logging. Assuming in the following that 5 to 10 % of the fractures are conductive, then:

$$P_{32c} = [5-10\%] P_{32g}. \quad (2.1)$$

The mean fracture frequency λ reported from NGU varies between 1 to 5 fractures per meter outside faulted zones. For a uniform distribution of fractures, the fracture intensity P_{32g} is roughly equal to 2λ , otherwise it varies between λ and 3λ (Dershowitz, 1993). Hence:

$$P_{32c} = [5-10\%] [1-3] [1-5] /m \quad (2.2)$$

giving:

$$P_{32c} = 0.05 - 1.5 \text{ fractures /m} \quad (2.3)$$

In the discrete fracture model the N-S oriented fractures are given the highest density, whereas the sub-horizontal fractures are given a low density due to their general tendency to close with depth (fracture closure with depth is not

available in the current version of Napsac). The intensities P_{32} for the different fracture sets have been adjusted by trials and errors to obtain roughly 50% of the fractures in the N-S direction, as reported by the site investigations. The following intensities have been used:

Set 1	(NS)	$P_{32c} = 0.12$ fracture / m
Set 2	(WNW-ESE)	$P_{32c} = 0.06$ fracture / m
Set 3	(Sub-horizontal)	$P_{32c} = 0.012$ fracture / m

2.3.4 Estimation of fracture shape and size

The shape and size of the fractures are highly uncertain. Most current conceptual fracture models assume either circular or rectangular fracture shapes. Dershowitz (1993), based on an observation of a large amount of trace maps in granite, tuff, schist, shale and chalk, emphasised that fractures should be rather polygonal in shape, as fracture growth is usually limited by intersection with other fractures. In Napsac, fractures can be rectangular in shape. In the following, in the absence of relevant data, the fractures are assumed to be square in shape.

In the absence of trace maps that could be used to calibrate the fracture length distribution, a "pragmatic geological judgement" was used to define the length of the fractures. For fractures not limited to any strata, Aarseth et al. (1997) showed that the most common length distributions of fractures is a power law, i.e. the number of fractures N with length greater than or equal to length L follows the relationship:

$$N \propto L^{-E} \quad (2.4)$$

where the exponent E varies between 1 and 2. A compilation of various data sets is shown in Fig 2.8, where the black line has a gradient of -2 for comparison. Dreuzy et al. (2001) showed theoretically and numerically that the hydraulic properties of power law length fracture networks can be classified into three types of simplified models depending on the value of the exponent. When the exponent E is higher than 3, then the classical percolation model based on a population of small fractures is applicable. For E lower than 2, on the contrary the hydraulic behaviour is controlled by the largest fractures of the network. Between these two limits, i.e. when E is between 2 and 3, a two-scale structure must be used.

In the following, the fracture lengths are assumed to follow a truncated power law distribution with an exponent of 2, and lower and upper length limits equal to 50 and 100 meters. According to Dreuzy et al. (2001), it is therefore anticipated that both large and small fractures control the hydraulic behaviour of the network. A sensitivity study is performed to investigate the influence of fracture length on the generated fracture network.

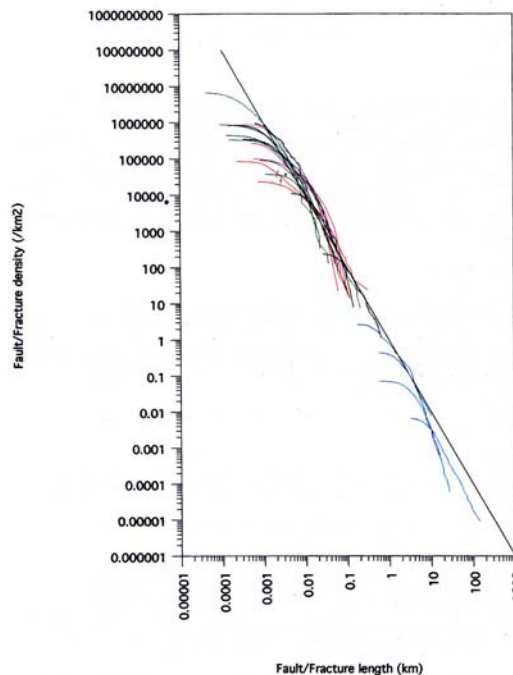


Fig. 2.8 Combined fracture trace length populations. Pale blue - Saudi faults; dark blue - Saudi joints; green - Hornelen joints; magenta Burren veins; red - Burren joints. Black line has a gradient of -2 for comparison. (from Aareseth et al., 1997)

2.3.5 Fracture distribution in space

A crucial parameter controlling the hydraulic property of the rock mass is the connectivity of the fracture network. The connectivity is controlled by fracture size, intensity and location. The fracture occurrence is usually assumed to be randomly through the rock mass (Priest, 1993), leading to a Poisson process, unless some form of correlation between fracture locations exists leading to clustering. Clustering can be modelled for instance with hierarchical models, where fractures are generated from previously defined fractures rather than from seeds located in space, or with varying intensity changing with distance from specific fractures (modelling of damage zone).

2.3.6 Summary of geometrical input parameters

The input parameters for generating the fracture network are summarised in the following table.

Table 2.2 Input parameters describing the fracture sets in the model.

Parameters	Set 1 (N-S)	Set 2 (WNW-ESE)	Set 3 (sub-horizontal)
Mean orientation (°)	0	115	0
Distribution	Uniform Spread 20	Uniform Spread 10	Uniform Spread 180
Mean dip angle (°)	90	90	10
Distribution	Uniform Spread 25	Uniform Spread 25	Uniform Spread 10
Length / Width (m)	Min: 50 Max: 100	Min: 50 Max: 100	Min: 40 Max: 60
Distribution	Power Law exponent: 2	Power Law exponent: 2	Power Law exponent: 2
Intensity P_{32c} (/m)	0.12	0.06	0.012

2.4 Estimation of hydraulic properties of fractures

2.4.1 Observation from Lugeon tests performed in Statens vegvesen borehole 1

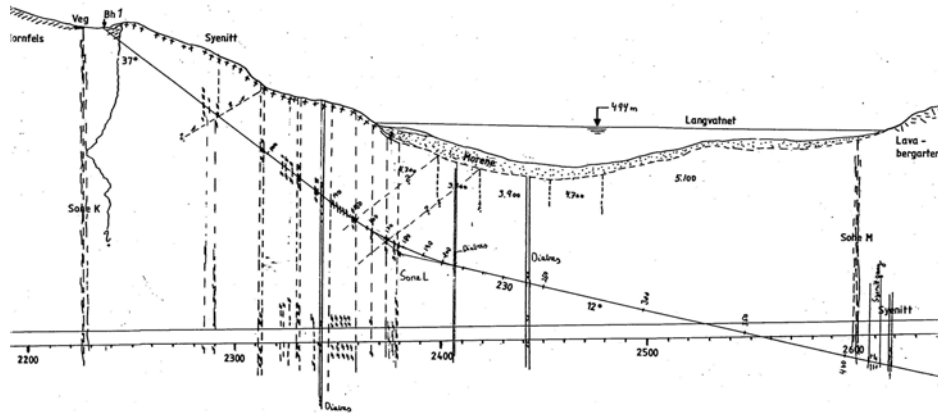
The fracture transmissivities are first estimated from Lugeon tests performed in borehole BH1 (see Fig.2.9 from Iversen, 1998). The borehole was drilled to assess the rock mass quality under Langvannet, as well as potential for leakage. The tests have been performed in 10m intervals throughout the whole borehole length.

One Lugeon is defined as the amount of water which can pumped into a section of a borehole during one minute under 10 bars overpressure. One Lugeon unit is approximately equal to 10^{-7} m/s (NGI, 1999). Assuming that the viscosity of the fluid is that of water at 10°C, the intrinsic permeability relates to the Lugeon unit as $1 \text{ Lugeon} \approx 1.3 \cdot 10^{-14} \text{ m}^2$.

The intrinsic permeability of the testing intervals has been calculated from the previous relation. As seen from Fig. 2.9, the permeability of the testing interval is variable along the borehole, and reflects somehow the degree of fracturing in the rock mass (i.e. high permeability for high fracture frequency). A rather poor correlation between permeability and fracture frequency is observed from a cross-plot of the two interpolated permeability versus fracture frequency. The average permeability for the whole borehole is roughly equal to $1.2 \cdot 10^{-14} \text{ m}^2$, where as the maximum value is $6.0 \cdot 10^{-14} \text{ m}^2 = 4.6 \cdot 10^{-7} \text{ m/s}$. According to the borehole log, this value is obtained for a single fracture, whose transmissivity T_f can be estimated as:

$$T_f = e_f K_f \approx H K_t \quad (2.5)$$

where e_f , K_f , H (=10m) and K_t are the fracture aperture, hydraulic fracture conductivity, height and hydraulic conductivity (m/s) of the testing interval, respectively.



Borehole 1

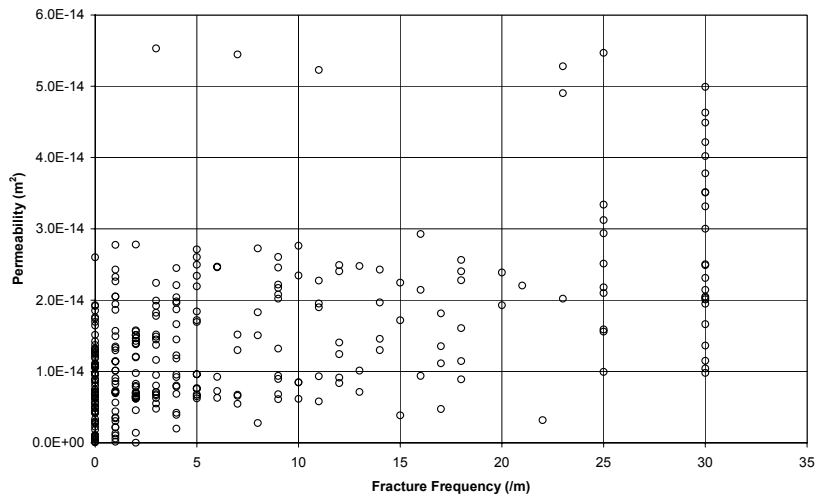
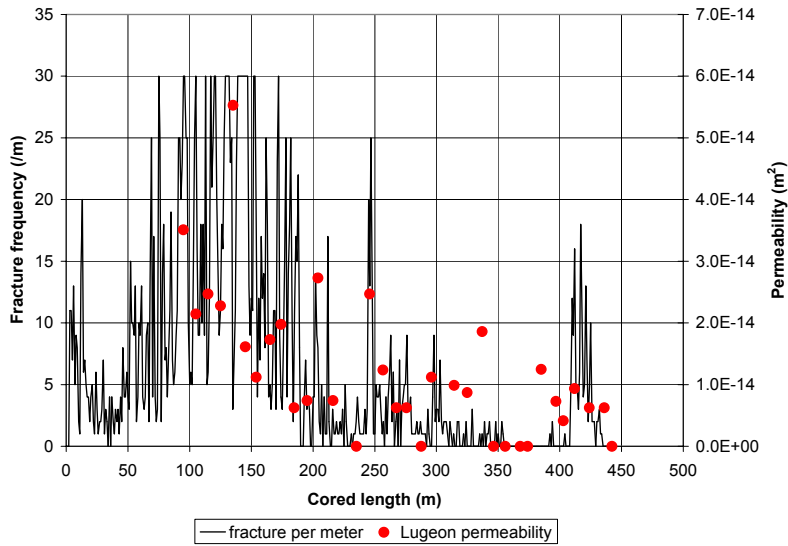


Fig. 2.9 Borehole profile and interpretation of Lugeon tests carried out by Statens vegvesen (data and profile from Iversen, 1998).

Based on the values reported above, the transmissivity of a conductive fracture T_f is assumed to be within the interval $[10^{-7} - 10^{-5}] \text{ m}^2/\text{s}$. Note that the transmissivity should be depth dependent, as fractures tend to close with depth. Since this option is not available in the current version of Napsac, the depth dependency is not considered. However, sub-horizontal fractures are given the lowest transmissivity value since they may close more easily at depth.

2.4.2 Observation from NGU boreholes

Hydraulic testing of 4 boreholes have also been carried out by NGU (2002). The boreholes have been inspected with optical viewers and geophysical logging methods. The tests show that the boreholes have a rather large water capacity, varying from 1 to $>15 \text{ m}^3/\text{hour}$ in the various boreholes. The conductive fractures as identified from pumping tests correlate fairly well with optical inspection of the boreholes.

2.4.3 Distribution of transmissivities

Based on the observation of a fracture system in Hornelen, Western Norway, Odling (1997) showed that the effective hydraulic aperture of a fracture, e , can be related to the fracture trace length l through the relationship:

$$e \propto l^{0.5} \quad (2.6)$$

This model predicts that length increases faster than effective aperture. Since transmissivity is proportional to the cube of the hydraulic aperture (see definition from Eq.1.2), it follows that the transmissivity T of the fractures is related to the fracture length through the relationship:

$$T \propto l^{1.5} \quad (2.7)$$

Hence it is assumed that the transmissivity values obey a power law distribution with an exponent equal to 1.5.

2.4.4 Fracture storativity

Transient flow modelling requires knowledge of fracture storativity. Such data do not exist for the site. Interpretation of NGU tests is not possible given the technical problems encountered during testing. Furthermore there is some doubt regarding the representativity of the tested intervals.

Consequently data available from published literature has been used. Niemi et al. (2000) suggested the following relationships:

$$\begin{aligned} S &= T \\ S &= 0.001 \sqrt{T} \\ S &= C \sqrt[3]{T} \end{aligned} \quad (2.8)$$

where C is a constant depending on the physical properties of water and aperture characteristics of the fractures. Note that in Eq.2.8, S is dimensionless and T is expressed in m^2/s .

The first relationship is based on the observation that in several cases summarised in Table 2.3, the diffusivity $\eta = T / S$ is in the order of 1. The second relationship is an empirical relationship proposed by Uchida et al. (1994) for the Äspö Hard Rock Laboratory in Sweden.

Table 2.3 Fracture storativity and transmissivity used in various fracture network simulation studies (from Niemi et al., 2000)

Reference (full reference in Niemi et al., 2000)	T ($\text{m}^2 \text{s}^{-1}$)	S	Site
Dershowitz et al. (1991)	$2 \cdot 10^{-7}$, $4 \cdot 10^{-7}$ (A)	10^{-8}	Stripa crown fractures
	$1 \cdot 10^{-8}$, $5 \cdot 10^{-6}$ (A)	10^{-8}	Stripa nonzone
	$2 \cdot 10^{-8}$, $4 \cdot 10^{-7}$ (A)	10^{-8}	Stripa fracture zone
	$1 \cdot 10^{-7}$, $3 \cdot 10^{-9}$ (A)	10^{-8}	Stripa fracture zone
	$1 \cdot 10^{-8}$, $1 \cdot 10^{-9}$ (A)		Stripa fracture zone
	$2 \cdot 10^{-8}$, $3 \cdot 10^{-5}$ (B)	$6 \cdot 10^{-9}$, ... $2 \cdot 10^{-4}$	
Long et al. (1992)	$2 \cdot 10^{-6}$, $1 \cdot 10^{-5}$ (C)	10^{-5}	Stripa fracture zone
Uchida et al. (1994)	$4 \cdot 10^{-7}$, $7 \cdot 10^{-6}$ (A)	$0.001 T^{0.5}$	Äspö nonzone
Winberg (1996)	-8.4, 0.9 (D)	$0.001 T^{0.5}$	Äspö nonzone
La Pointe et al. (1995)	$9 \cdot 10^{-7}$, $5 \cdot 10^{-6}$ (A)	10^{-6}	Äspö nonzone

Table footnotes:

(A): lognormal distribution. Mean and standard deviation indicated

(B): range of values indicated

(C): channel conductance indicated. units in $\text{m}^3 \text{s}^{-1}$

(D): mean and standard deviations given in \log_{10} space

The third relationship comes from the definition of storativity, and assuming that the medium is incompressible and the porosity equal to 1 in a fracture, one obtains:

$$S = \rho g e_s c_w \quad (2.9)$$

where c_w is the compressibility of water ($\text{m kg}^{-1} \text{s}^2$), and e_s the aperture of the fracture controlling the storage properties. e_s is usually larger than the hydraulic aperture, with one order of magnitude (Niemi et al., 2000). Using a ratio e_s / e equal to 10 gives a value of the constant $C = 4.4 \cdot 10^{-7} \text{ s}^{1/3} \text{ m}^{-2/3}$ in Eq. 2.8. The reader is referred to Tsang (1992) for a comprehensive overview and discussion regarding the different equivalent apertures defined from hydraulic and tracer tests.

In the following, in the absence of data, the storativity model is assumed to follow the following relationship (default in Napsac):

$$S = 0.25 T^{0.74} \quad (2.10)$$

The 4 storativity models given by Eqs. 2.8 and 2.10 are shown in Fig. 2.10. for comparison.

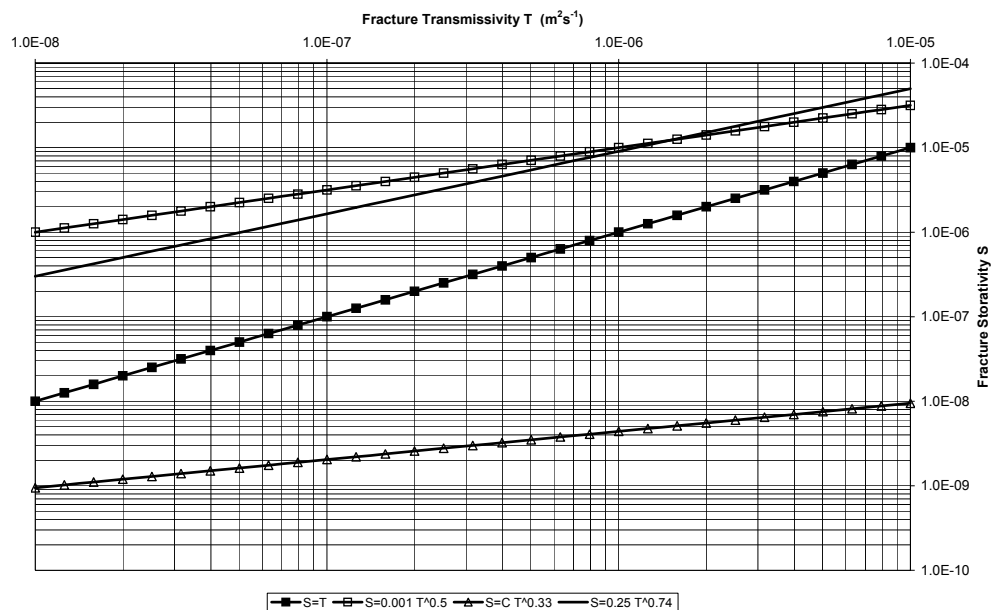


Fig. 2.10 Comparison between fracture storativity models

2.5 Hydraulic calibration of fracture networks

In this section, the Lugeon tests carried out by Statens vegvesen (Iversen, 1998) are used in an attempt to calibrate the hydraulic transmissivities of the stochastic fracture network so that the local hydraulic properties of the fracture network are statistically the same as the real network. Note that this supposes that the assumption of ergodicity¹ yields for the medium.

The approach is similar to that used by Cacas et al. (1990) and more recently by Niemi et al. (2000). The basic procedure is as follows: 1) on the basis of the statistics of the fracture geometry presented in Table 2.2, 50 realisations of different but statistically similar fracture networks are generated in a 50 m x 50 m x 50 m cube. 2) In each network realisation, a Lugeon test is performed into a 10m interval. A constant head of 100m is imposed in the injection interval, whereas the boundaries of the cubes are set to hydrostatic conditions. The duration of the test is taken as 10 minutes. 3) The resulting statistics of the simulated well tests are compared with the corresponding statistics from the

¹ The hypothesis of ergodicity means that the geometry and spatial distribution of local hydraulic properties of the real medium can be considered as the result of a random realisation according to a probability law stationary in space.

measured data. 4) The distributions of individual fracture transmissivities are adjusted until a gross agreement between the measured and modelled statistics is achieved.

Note that as an approximation, the inclination of the borehole was taken as 45 degrees in the modelling exercise where as in reality the inclination varies along the borehole trajectory. Hence the number and types of fractures intersected vary in space because of the varying inclination. In addition, only the background fracture network is considered, and no deterministic fault zone is introduced in the model. This might introduce a limitation in the comparison exercise, as the most transmissive intervals are related to presence of fault zones.

The model geometry, the borehole and one fracture network realisation is shown in Fig.2.11 - left. The fractures intersecting the production interval are shown in Fig.2.11 - right, together with a trace map of the fractures on a horizontal plane at injection level. The fractures are colour-coded according to their family set.

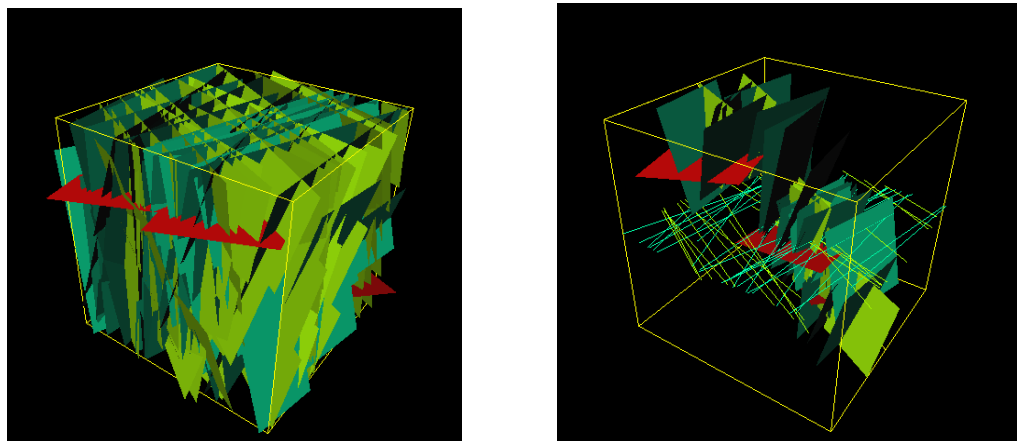


Fig. 2.11 Example of network realisation used in the 10-m scale well test simulation. The cube dimensions are 50m x 50m x 50m. a) left: fracture network b) right: Intersection of fractures and production interval in borehole. A trace map of the fracture network on a horizontal plane crossing through the production interval is also shown in the figure.

The statistics from the Lugeon tests performed in Borehole 1 (BH1) are presented in Fig.2.12, where the logarithm of the injection flow rates are classified in a histogram. The flow rates obtained in the injection interval vary over three orders of magnitude. Note that circa 20% of the injection intervals do not show any leakage.

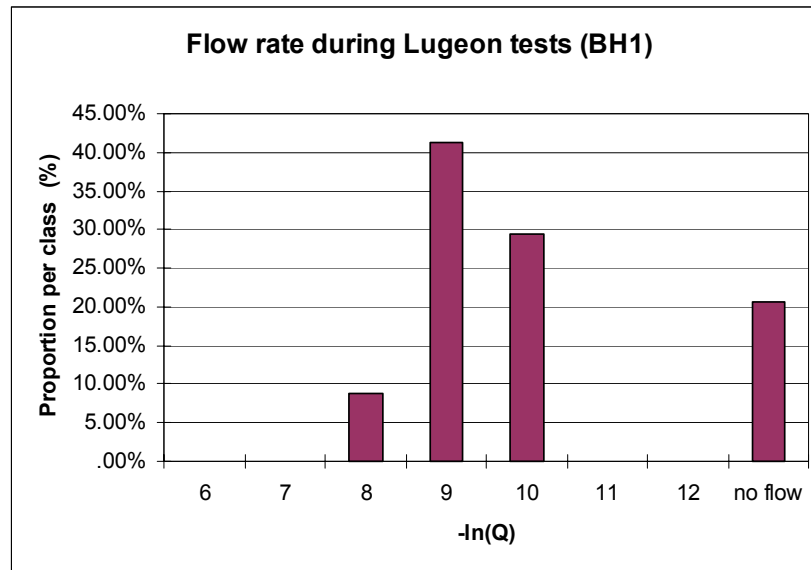


Fig. 2.12 Histogram of injection flow rates (m^3/s) obtained during Lugeon testing in Statens vegvesen Borehole 1 (BH1)

In Fig.2.13, the same data are presented together with the results from well pressure tests performed in stochastically generated discrete fracture networks. For plotting purposes, non leaking intervals have been assigned a default value $-\ln(Q)$ equal to 13. Different fracture densities have been considered:

- a highly dense fracture network, characterised by a conductive fracture intensity P_{32} equal to 1.2, 0.6 and 0.12 /m respectively for Set 1, 2 and 3. (Case P32H in Fig.2.13)
- a moderately dense fracture network, characterised by a conductive fracture intensity P_{32} equal to 0.24, 0.12 and 0.024 /m respectively for Set 1, 2 and 3. (Case P32M in Fig.2.13)
- a sparsely fractured network, characterised by a conductive fracture intensity P_{32} equal to 0.12, 0.06 and 0.012 /m respectively for set 1, 2 and 3. (Case P32L in Fig.2.13)

For the highly dense fracture network, two transmissivity distributions are considered:

- T1: Sets 1,2: truncated power law distribution: exponent equal to 1.5, minimum and maximum bounds equal to 10^{-7} and 10^{-5} m^2/s . Set 3: constant transmissibility equal to 10^{-7} m^2/s .
- T2: Sets 1,2: truncated power law distribution: exponent equal to 1.5, minimum and maximum bounds equal to $5 \cdot 10^{-8}$ and 10^{-6} m^2/s . Set 3: constant transmissibility equal to $5 \cdot 10^{-8}$ m^2/s .

For the moderately dense and sparsely fractured media, the transmissivity distribution T1 is used.

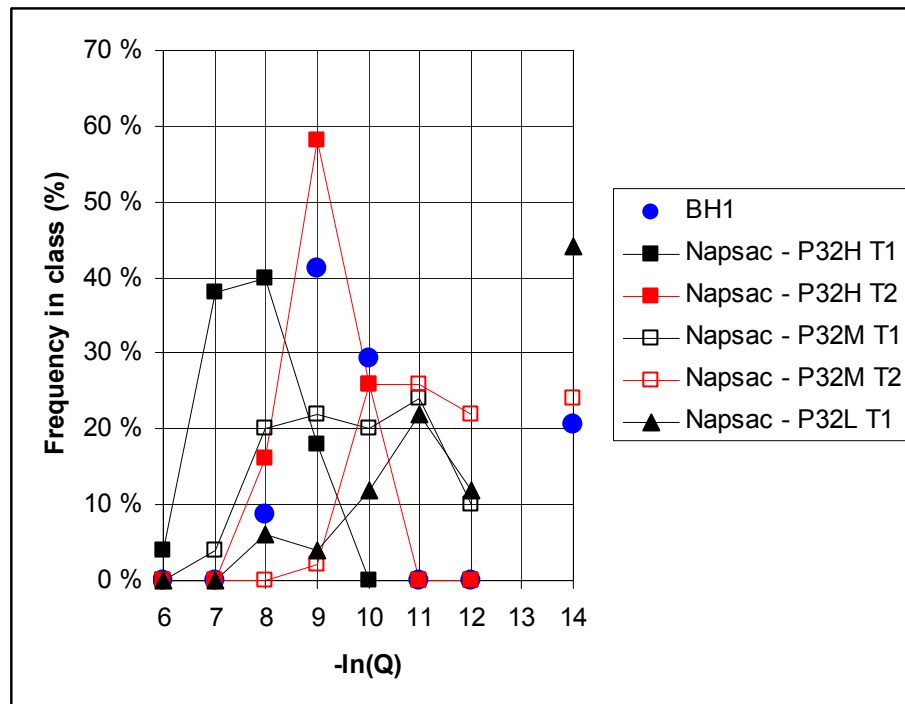


Fig. 2.13 Histogram of injection flow rates obtained during Lugeon testing. Data from borehole 1 (BH1) are indicated with blue dots. Data from Napsac are indicated with plain lines, corresponding to three fracture intensities P32 (High percolating network, Medium and Low), and two different transmissivity distributions. No flow data is arbitrarily set to $-\ln(Q)=14$

The results shown in Fig.2.13 indicate that:

- It is difficult to match both the occurrences of test intervals with high flow rates and test intervals without fractures. The main reason is that the occurrence of test intervals with high flow rates is most probably due to the intersection with faults, which are not considered in the numerical simulation of the Lugeon tests.
- Only the moderate and sparsely fractured network predict the occurrence of borehole injection intervals free from fractures (i.e. without any leakage). A good agreement in terms of occurrence of intervals free from fractures is obtained for a moderate fractured network.
- If one disregards the data points for highly leaking intervals, a reasonable agreement can be found between the flow rates histogram inferred for the stochastic numerical model and the field data by considering a moderate fractured network and a narrow range of transmissivity distribution (model P32M T2 in Fig. 2.13). However the presence of faults should reduce the occurrence of test intervals "free from fractures", so that a sparsely fractured network might be closer to real conditions.
- Reducing the fracture intensity leads to a broader range of flow rates, with a lower frequency in each class. Increasing the fracture intensity

leads to a narrower range of flow rates, with higher frequency in each class.

2.6 In situ and boundary hydrogeological conditions for the site

Based on general knowledge of groundwater flow it is assumed that the general flow pattern within the model area will more or less follow the topography. This means that there is a groundwater gradient of 0.25 between the topographical height in the west and down to the Langvatnet in the east.

Due to the presence of major weakness zones and horizontal fractures, there is however some uncertainty regarding the position of the water table in the model and the influence of Langvatnet (lowest head).

Shallow borehole tests performed by Jordforsk (Snilsberg & Kløve, 2001) in the model area before tunnel excavation have shown that outside the major weakness zone K in the hornfels, the water table coincides with the rock surface (wells B1 and B2), whereas inside the weakness zone the water table varies. The deep water table seems to be at the same level as Langvatnet, the lake located 150 m to the east of the weakness zone.

The annual observed precipitation for the area varies between circa 200 mm/year (2001, normal year) to about 800 mm/year (2000, wet year). The effective infiltration recharge for the area is hard to estimate. Net infiltration values into the rock mass between 10 to 25 % of the annual precipitation are suggested (Kløve & Kværner, 2001).

3 PREDICTION OF TUNNEL INFLOWS FROM FRACTURE NETWORK MODELLING

3.1 Introduction

In this section, the effect of the tunnel on the groundwater flow in the region of interest is investigated. The rock mass is modelled as a stochastic fracture network based on the parameters presented in Section 2. As outlined in Section 2, the determination of several critical input parameters for the discrete network model is highly uncertain. Such parameters concern for instance the fracture length, the transmissivity of deterministic faults, the fracture characteristics in the hornfels, but also the initial hydrological conditions in the area, and the proper choice of boundary conditions to be applied in a numerical model. Consequently, several hypotheses concerning these parameters have been put forward. In order to test the sensitivity of the leakage prediction to these hypotheses, several models have been investigated. The models are described in details in the next section. First a 2D continuum model is used to investigate the influence of model size on the tunnel leakage. Characteristic

times involved in the pressure diffusion are also put forward. Then the Napsac model is presented together with the flow results.

3.2 Estimation of model size and characteristic time scales involved in transient flow

3.2.1 Effect of model size

Flow modelling in discrete fracture networks can be time consuming when the size of the model is large. Consequently a compromise must be found between model size and interaction with boundaries. In the following the effect of model size on tunnel leakage is quickly investigated in two dimensions with a continuum model (Figure 3.1). Only half of the model geometry is modelled, due to symmetry. A worst case scenario is studied in order to assess the minimum size of the numerical model, therefore a higher value of the permeability is chosen. The main assumptions are:

- the rock mass is assumed continuous and homogeneous, characterised by its porosity n ($n=0.3$) and isotropic hydraulic conductivity K ($K=10^{-6}$ m/s). This value should be compared to a maximum conductivity of $4.6 \cdot 10^{-7}$ m/s interpreted from the Lugeon tests in Borehole 1 (Section 2.4.1).
- the tunnel radius is equal to $R = 3,9$ m. The pressure is fixed and equal to zero at the tunnel face. The tunnel depth D is equal to 100 meters for all models. The model size W is varied between 500 and 1000 meters.
- groundwater flow is linear. Steady state conditions are considered. A precipitation recharge q (in $\text{m}^3/\text{s}/\text{m}^2$) is applied at the top boundary of the model. Hydrostatic conditions are applied at the lateral boundaries.

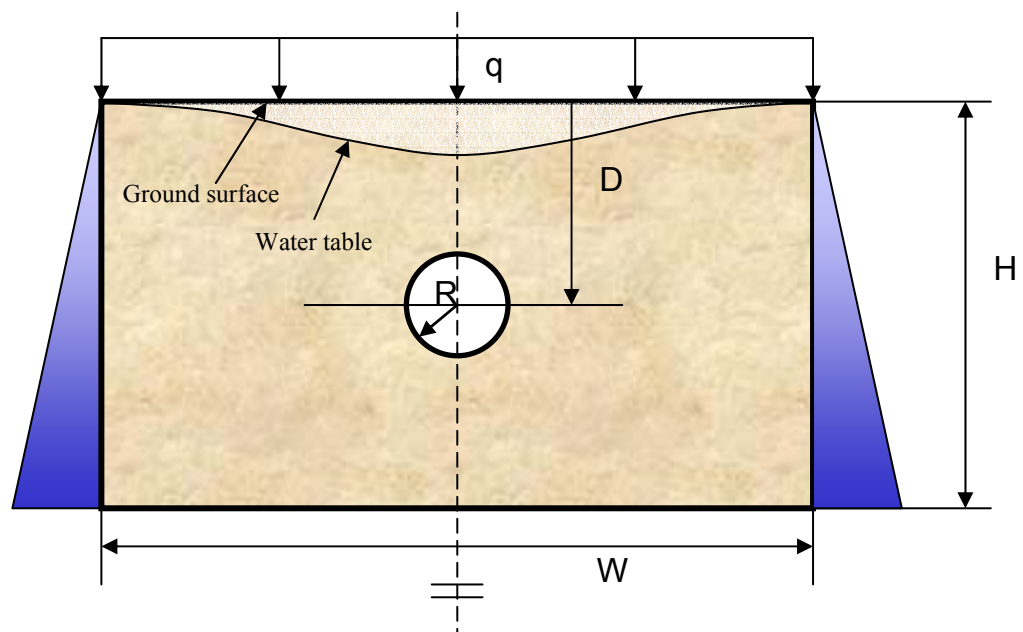


Fig. 3.1 Schematic representation of a 2D model to investigate the effect of boundary conditions on prediction of tunnel leakage.

Under steady state conditions, the water table is established as shown in Fig.3.2. The distance from the tunnel to the water table is influenced mainly by the width of the model. The tunnel leakage from the different models is given in Table 3.1.

Table 3.1 Results from numerical analyses with continuum model

Model Name	Width W (m)	Height H (m)	Inflow in tunnel (l/min/100m)	Comment
w1	500	175	504	Reference size Recharge $q = 10^{-9} \text{ m}^3 \text{ s}^{-1} / \text{m}^2$
w5	500	175	504	Same as w1 but different grid
w2	1000	300	444	Effect W, H Recharge $q = 10^{-9} \text{ m}^3 \text{ s}^{-1} / \text{m}^2$
w3	1000	175	288	Effect W Recharge $q = 10^{-9} \text{ m}^3 \text{ s}^{-1} / \text{m}^2$
w4	500	300	660	Effect H Recharge $q = 10^{-9} \text{ m}^3 \text{ s}^{-1} / \text{m}^2$
w6	500	175	882	Constant water table in model - no recharge
w7	1000	300	948	Constant water table in model - no recharge

As shown from Table 3.1, the grid size has a pronounced effect on the total leakage into the tunnel (where as the grid itself does not influence as such). The predictions from the numerical model were also checked against an analytical solution for the case of constant water table above the tunnel. The first order solution proposed by El Tani (1999) is used to predict the amount of water which flows into the tunnel. The inflow rate is given by:

$$Q_o = 2\pi K \frac{h}{\ln \frac{2h}{r}} \quad (3.1)$$

where h is the distance from the tunnel centre to the water table, r the tunnel radius and K the hydraulic conductivity. With the above values, Eq. (3.1) gives a leakage rate equal to 960 l/min per 100m tunnel when $h=100\text{m}$. This solution is more or less obtained if the boundaries of the model are far enough, as seen in run **w7**. The results from run **w6** show that the size of the model has some effect on flow prediction even for the case of a constant water table, although the difference remains small (less than 10%). In both cases, water inflow into the tunnel is much higher than in the cases where the water table is draw down towards the tunnel, which indicates that Eq. (3.1) over-estimates the inflow into a tunnel.

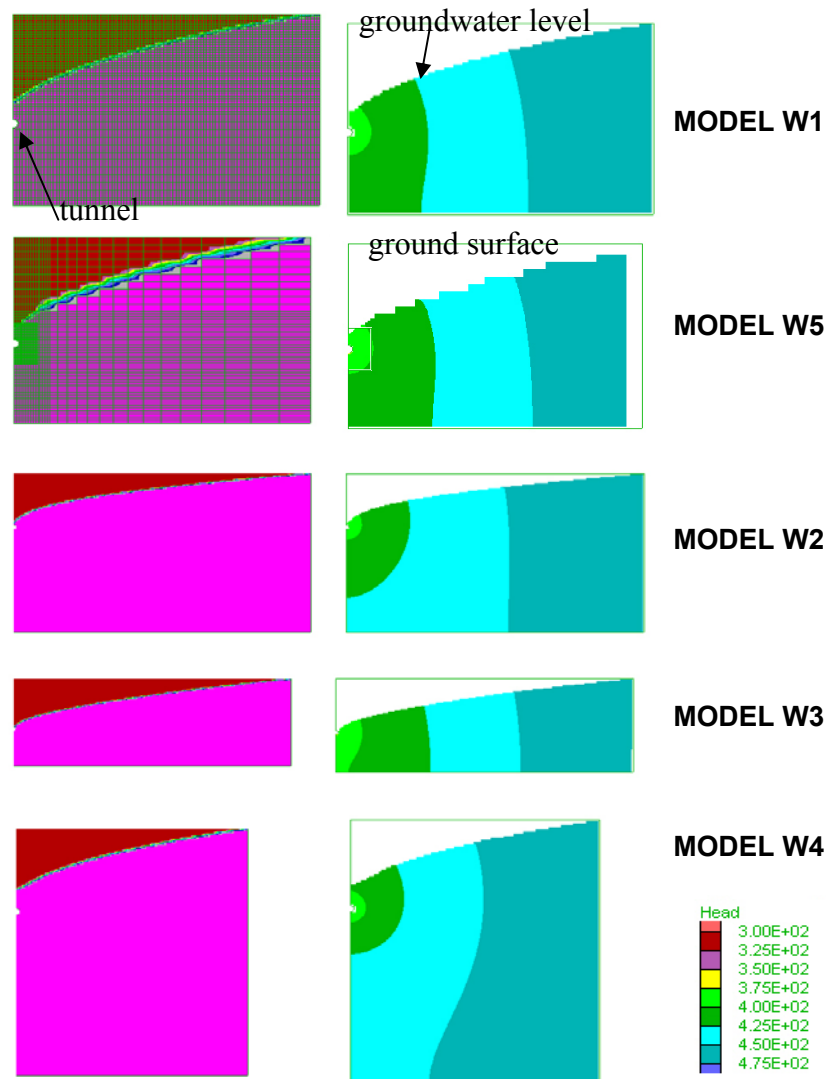


Fig. 3.2 Effect of grid and model size on water table and total head. NB: Dimension scale varies from plot to plot

3.2.2 Characteristic times involved in unsaturated flow

In the numerical simulations presented above the calculation time required for the phreatic surface to reach its steady state position has been decreased by reducing the mean value of fluid bulk modulus. Hence the results illustrate the effect of model size on the final position of the phreatic surface. In nature there are two distinct time scales associated with unsaturated flow, if one ignores additional effects associated with mechanical adjustments or natural sealing of fractures due to transport of fines. There is a *short* time scale associated with the adjustment of the flow field to the given boundary conditions, including the current location of the phreatic surface. Such a time scale is controlled by the fluid storage n/K_w , where n is the rock porosity and K_w the bulk modulus of water. Such a time scale is in practise in the order of minutes or hours. Over the *long-term* the phreatic surface adjusts its location in response to unbalanced

flow around partially saturated zones. Such a phenomenon occurs over days, weeks or years, as controlled by the phreatic storage. Characteristic times of the two phenomena for the numerical problem depicted above can be given as:

Short term behaviour:

$$T_s = \frac{\left(\frac{W}{2}\right)^2}{k} \frac{n\rho_w g}{K_w} \quad (3.2)$$

where $W/2$ is the half width of the model (i.e. the average length of the flow path through the medium), n the rock porosity, k the hydraulic conductivity, ρ_w the water density, g the acceleration of gravity, and K_w the bulk modulus of water.

Long term behaviour:

$$T_l = n \frac{\left(\frac{W}{2}\right)^2}{k} \left(\frac{\rho_w g}{K_w} + \frac{1}{H} \right) \quad (3.3)$$

where H is the height of the model available for fluid storage.

Assuming that

$$\begin{aligned} n &= 0.3 \\ K_w &= 2 \cdot 10^9 \text{ Pa} \\ \rho_w g &= 10^4 \text{ N/m}^3 \end{aligned}$$

the characteristic times T_s and T_l are given in Tables 3.2 and 3.3 for various values of half-width $W/2$, height H and hydraulic conductivity k .

This behaviour can be recognised by comparing a typical pressure history with histories of inflow and outflow: the pressure history shows convergence to a steady value, but inflow does not balance outflow, because there is unaccounted flow in or out of the partially saturated zones.

As seen from Tables 3.2 and 3.3, the long term steady state condition is reached after some couple of years (or more) depending on the model width. Hence for practical purposes, steady state stabilisation of the phreatic surface does not occur around the tunnel and a transient analysis should be considered.

Table 3.2 Characteristic time for transient flow behaviour - effect of geometry. Hydraulic conductivity $k = 10^{-6}$ m/s.

Model Height H (meters)	Model Width W/2 (meters)	Short term T_s (days)	Long term T_l (days)
175	250	1	1241
175	500	4	4965
300	250	1	724
300	500	4	2898

Table 3.3 Characteristic time for transient flow behaviour - effect of permeability ($H=175$, $W/2=250$)

Hydraulic conductivity k (ms^{-1})	Short term T_s (days)	Long term T_l (days)
10^{-4}	0	12
10^{-5}	0	124
10^{-6}	1	1241
10^{-7}	11	12412
10^{-8}	109	124116
10^{-9}	1090	1241164

3.3 The Napsac numerical model

3.3.1 The modelling region

The modelling region defined from Fig.2.2 is schematically shown in Fig.3.3. The modelling region is a parallelepiped oriented North South with an horizontal area of 550 m x 550 m. The top surface follows the topography and tilts down to the east with a 0.25 gradient. The tunnel is running approximately east-west through the model.

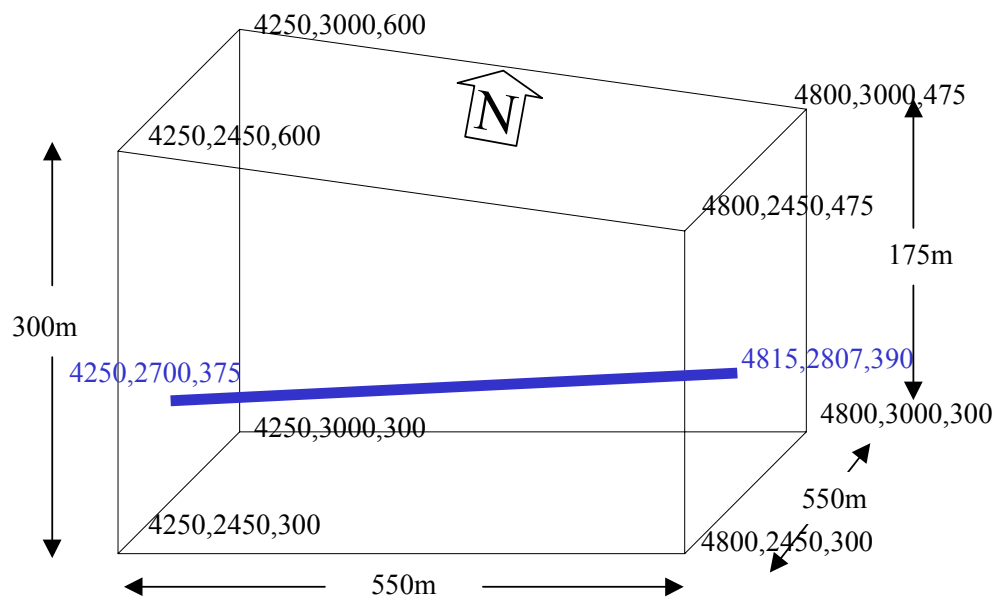


Fig. 3.3 The bounding box of the discrete fracture network model. The coordinates are based on the last 4 digits of the UTM coordinates for x and y and $m.a.s.l$ for z . The start and end points of the tunnel (in blue) are also indicated.

3.3.2 The tunnel

The tunnel is excavated with a T8,5 profile, giving a cross-sectional area of 46,9 m². In the numerical model, the tunnel is represented as a cylindrical well with an equivalent radius $r = 3,86\text{m}$ giving the same sectional area as the real tunnel geometry. The tunnel inner boundaries are set to the atmospheric pressure.

3.3.3 Initial and boundary conditions

Boundary conditions are an important part of the numerical model as they may influence the results, especially when the model area is rather small compared to the main geological structures. Based on general knowledge of groundwater flow it is assumed that the general flow pattern is following the topography. Further, observations of groundwater level in wells gives information about the initial groundwater situation in the model area and may be used to calibrate the boundary conditions before tunnel excavation.

Different boundary conditions have been investigated (Fig. 3.4). These are:

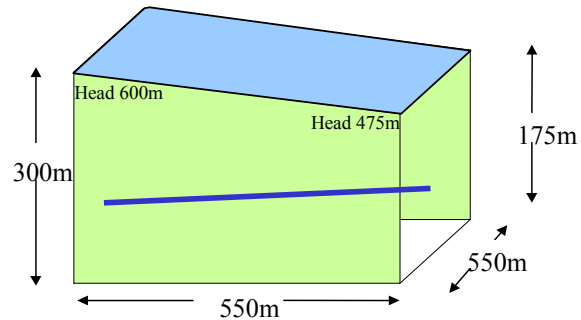
- BC1: a constant head boundary condition is set on the northern and southern boundary, representing the groundwater gradient in the area. The whole model area is assumed to be under the groundwater table.
- BC2: the boundary conditions have been modified in order to reflect better groundwater observations from wells. The northern and southern boundaries have been given a head gradient from the topographical height in the west and down to zone K. A constant head is set between zone K and Langvatnet based on observations from Jordforsk wells B3 and B4 suggesting that the groundwater level in zone K is close to Langvatnet.
- BC3: a constant head boundary is set to a part of the top surface to represent a constant water level in Langvatnet. With this model, the precipitation recharge has been calibrated in order to obtain a realistic initial groundwater table in the model. It was found that an effective infiltration equal to 10 % of the total infiltration was more realistic than 25 %.

On the top surface an inflow flux equal to $6.0 \cdot 10^{-9}$ or $2.5 \cdot 10^{-9} \text{ m}^3 \text{ s}^{-1} / \text{m}^2$ is imposed to account for precipitation recharge. These figures are based on a precipitation of 800 mm/year, out of which 25% or 10% are infiltrating into the rock mass. Boundary surfaces that are not given any specific value are considered as no flow boundaries.

Boundary conditions 1

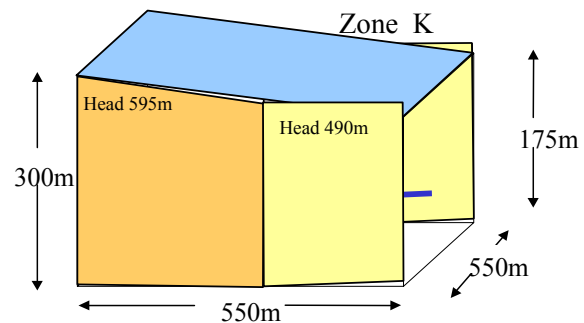
North and south: head gradient following the topography

Top: Inflow 6.0×10^{-9} m/s

**Boundary conditions 2**

North and south: head gradient following the topography down to zone K, constant head between Langvatnet and zone K

Top: Inflow 2.5×10^{-9} m/s

**Boundary conditions 3**

Top (blue): Inflow 2.5×10^{-9} m/s

Top (pink): constant head Langvatnet

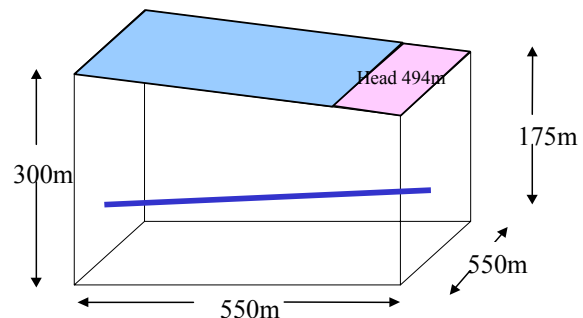


Fig. 3.4 Boundary conditions used in the numerical models

3.4 Sensitivity analysis

3.4.1 Effect of background fractures (stochastic)

The background fractures consist of three fracture sets with different orientation and density. The fracture length is the most uncertain parameter for the fracture sets, as it is difficult to infer from borehole logs. Sets with different length and length distribution have been tested to quantify their influence in total inflow in the tunnel. Boundary conditions BC-1 are used. The results are outlined in Fig. 3.5, which shows the fracture network on the top surface, together with total inflow per 100 m of tunnel. The four networks investigated correspond to:

- Net1: uniform fracture length distribution
- Net2: truncated power law fracture length distribution –longer fractures than Net3
- Net3: truncated power law fracture length distribution

- Net4: truncated power law fracture length distribution –higher density

For all cases, the transmissivity distribution of fracture sets 1 and 2 follows a truncated power law, with a minimum and maximum value respectively equal to 10^{-7} m²/s and 10^{-5} m²/s, and an exponent equal to 1.5. The transmissivity of fractures in Set3 is constant equal to 10^{-7} m²/s.

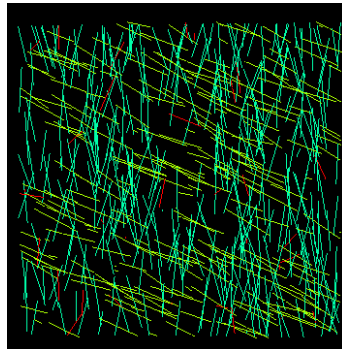
As shown in Fig.3.5, the variation in total flow is moderate, although local variation in flow occurs. For the same fracture length and density there is no difference between uniform fracture length distribution (Net1) and truncated power law fracture length distribution (Net 3). Increasing the fracture length from max 100m to max 200m gives a minor increase in inflow, whereas a 0.02 /m increase in fracture density gives a slightly higher increase in inflow. This indicates that the fracture density is a sensitive parameter for flow.

The background fractures are stochastically generated with the use of a seed number. By varying the seed, different network realisations are generated, although the networks are all statistically equivalent. As the inflow in the tunnel depends on the number of fracture intersection with the tunnel, each realisation gives a different inflow.

As an example, fracture network Net4 depicted in Fig. 3.5 has been generated with 10 different seeds. The tunnel inflow is shown in Fig. 3.6 for all realisations. A 25% variation around a mean value is obtained. This variation is similar to that obtained when various length distributions were tested in Fig 3.5.

3.4.2 Effect of faults – fracture zones (deterministic)

Deterministic faults are introduced in the model to represent fault and faults zones whose position is known. However, fault and fault zones are usually associated with a damage zone in which high fracturing occurs. In the following the effect of a damage zone is illustrated. The fracture network NET 4 is considered. Fig. 3.7 illustrates the difference between two representations of fault zones as plane or zone of high fracture intensity. The difference between the two models is minor.



Net 1

Length distribution: Uniform

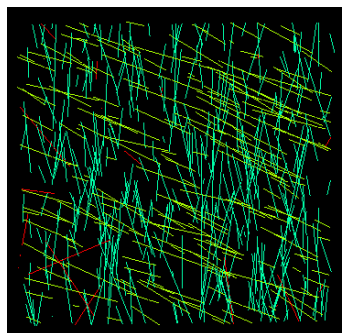
Set1-2: Mean 75 m, Spread 25 m

Set3: Mean 50 m, Spread 10 m

Density: Set1: 0.1, Set2: 0.05, Set3: 0.01

Fractures: 3224

Q = 48 l/min/100m



Net 2

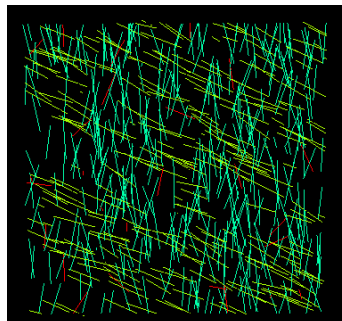
Length distribution: Truncated Power Law

Set1-3: Min: 25m, Max: 200m, e: 2

Density: Set1: 0.1, Set2: 0.05, Set3: 0.01

Fractures : 2539

Q = 50 l/min/100m



Net 3

Length distribution: Truncated Power Law

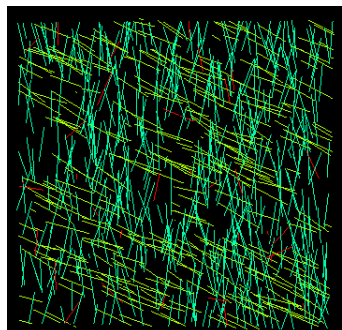
Set1-2: Min: 50m, Max: 100m, e: 2

Set3: Min: 40m, Max: 60m, e: 2

Density: Set1: 0.1, Set2: 0.05, Set3: 0.01

Fractures: 2784

Q = 48 l/min/100m



Net 4

Length distribution: Truncated Power Law

Set1-2: Min: 50m, Max: 100m, e: 2

Set3: Min: 40m, Max: 60m, e: 2

Density: Set1: 0.12, Set2: 0.06, Set3: 0.012

Fractures: 3347

Q = 64 l/min/100m

*Fig. 3.5 Influence of background fracture network on total inflow in tunnel.
The fracture network geometry is viewed from the top surface.*

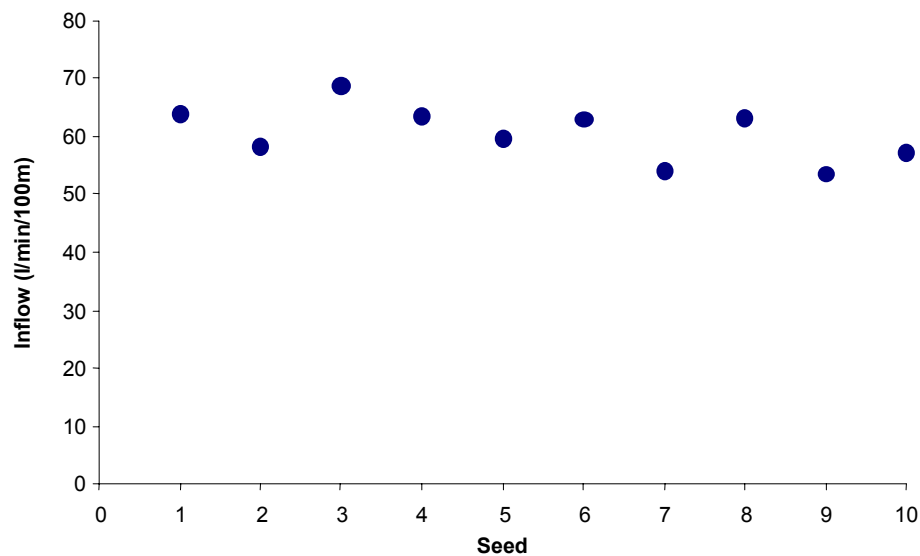
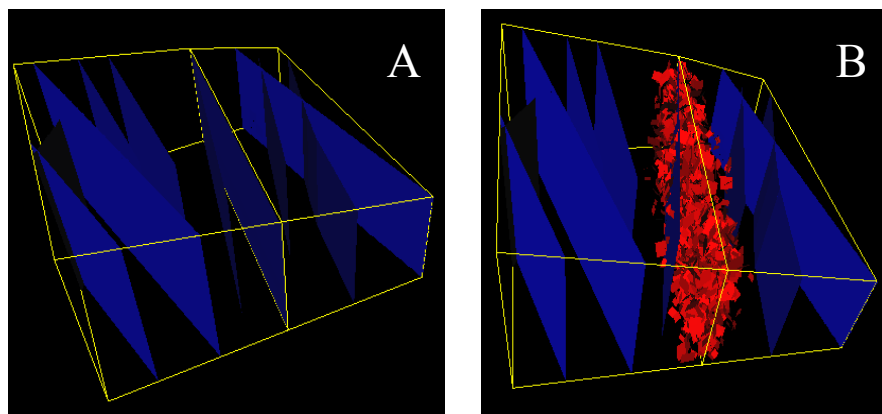


Fig. 3.6 Inflow variation for background fractures in NET4 tested for 10 different realisations



NET 4 with 12 deterministic faults
 $Q = 176 \text{ l/min/100m}$

NET 4 with 11 faults and 1 damagezone
 $Q = 162 \text{ l/min/100m}$

Fig. 3.7 All faults modelled as planes with a given transmissivity (A) and a fault modelled as a zone of higher fracture intensity (B).

3.4.3 Effect of transmissivity distribution

A crucial parameter in the estimation of tunnel inflow is the hydraulic properties of fractures and faults. In this section three cases are investigated, which correspond to low, medium and high maximum values of fracture transmissivity (Table 3.4). The transmissivity distribution is (truncated) power law with an exponent equal to 1.5. Only the maximum value is varied. It is

assumed that the transmissivity of a deterministic fault is equal to the highest value.

The inflow is illustrated in Fig. 3.8 along the tunnel. The upper figure gives an average value for each 100 m interval, where as the lower figure gives the inflow variation along the tunnel. As seen from the figure, the inflow is controlled mainly by the deterministic faults, where local inflow peaks are observed. Note that since the transmissivity distribution follows a power law, very few stochastic fractures have a high transmissivity, so that for a high maximum value of transmissivity, the background fractures do not contribute significantly to leakage into the tunnel.

Table 3.4 Transmissivity values used in sensitivity analysis

Run Names	Background fractures		Deterministic faults
	T_{\min} (m ² /s)	T_{\max} (m ² /s)	T_{faults} (m ² /s)
NET4-F	10^{-7}	10^{-5}	10^{-5}
NET4_3-F3	10^{-7}	10^{-4}	10^{-4}
NET4_4-F4	10^{-7}	10^{-6}	10^{-6}

3.4.4 Effect of boundary conditions and permeability contrast

Four different models are presented to illustrate the effects of boundary conditions and flow regime on the groundwater flow and tunnel leakage. The transmissivity value of deterministic fault planes is the same for all models, and varies according to rock type: hornfels, syenite, transition zone K (Table 3.5). Models 1 and 2 are identical except that in Model 2, deterministic faults have been truncated 50 m from the model boundaries. Model 3 differs from the use of boundary conditions BC-3. No field data is available to characterise the properties of the fractures in the hornfels formation, as all the boreholes pertain mostly to the syenite formation. However, based on geological experience, it is expected that the characteristics of fracturing in these two formations is quite different, more abundant but tighter fractures being formed in hornfels. Consequently, in Model 4, the transmissivity of background fractures is decreased by an order of magnitude in the hornfels region to investigate the effect of permeability contrast between the two formations.

Table 3.5 Effect of boundary conditions – description of models. NB: in all models, the transmissivity of background fractures follows a truncated power law distribution with an exponent equal to 1.5.

Model Name	Boundary conditions	Min, Max Transmissivity of background fractures (m ² /s)		Transmissivity of deterministic fault planes (m ² /s)		
		Hornfels	Syenite	Hornfels	Syenite	Zone K
Models 1/2	BC-2	10^{-7} - 10^{-5}	10^{-7} - 10^{-5}	10^{-6}	10^{-5}	10^{-4}
Model 3	BC-3	10^{-7} - 10^{-5}	10^{-7} - 10^{-5}	10^{-6}	10^{-5}	10^{-4}
Model 4	BC-2	10^{-8} - 10^{-6}	10^{-7} - 10^{-5}	10^{-6}	10^{-5}	10^{-4}

The results from Models 1 to 4 are presented in Figs. 3.9 to 3.12. The initial pressure distribution in Models 1 and 2 (Figs. 3.9A and 3.10A) gives an unrealistic initial flow pattern with water flowing in from the sides in the upper part of the model and out on the sides in the lower part of the model. However, the steady state pressure solution shows the expected reduction in pressure towards the tunnel. In Model 3, a head boundary condition is only imposed on the area corresponding to Lake Langvatnet. This model shows better initial pressure conditions with water flowing from the high areas down to the lake Langvatnet (Fig. 3.11A). The inflow into the tunnel in Model 3 is similar to Models 1 and 2 at day 1, but under steady state conditions most of the modelled region is emptied for water.

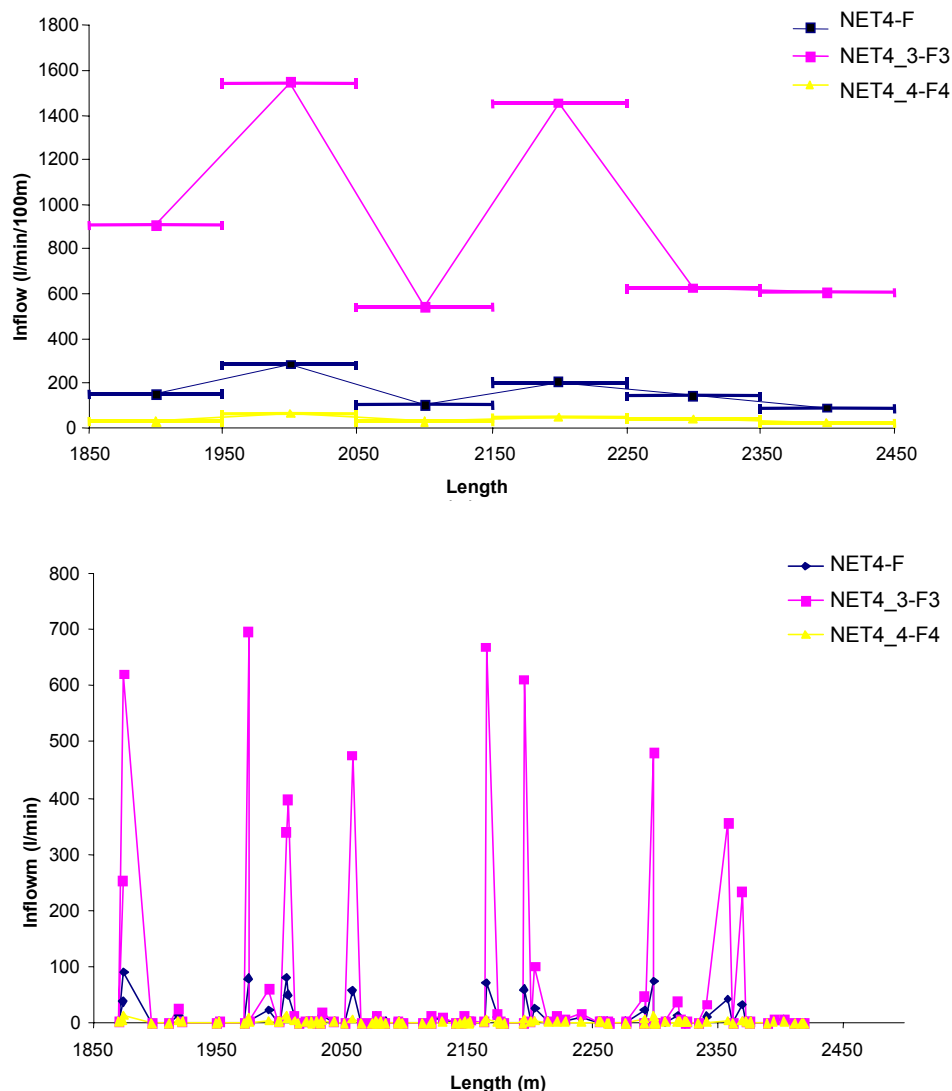


Fig 3.8 Inflow in the tunnel (bottom) and inflow per 100m (top) for low transmissivity (yellow), intermediate transmissivity (blue) and high transmissivity (pink). Input values are given in Table 3.5.

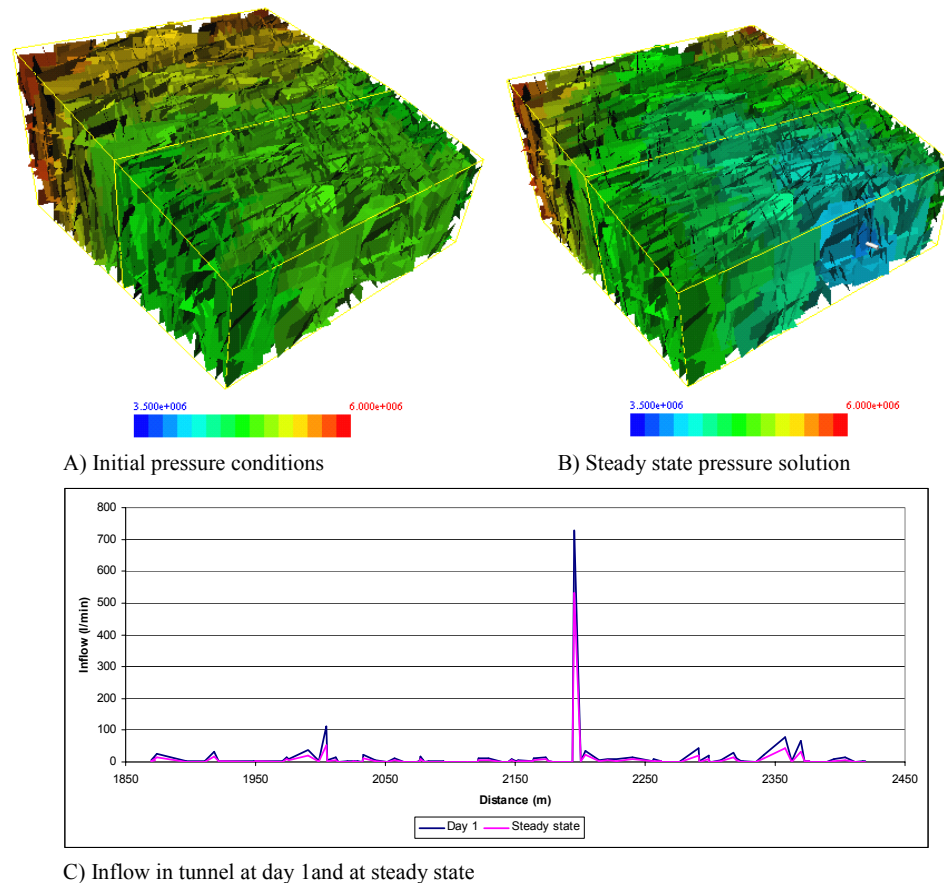
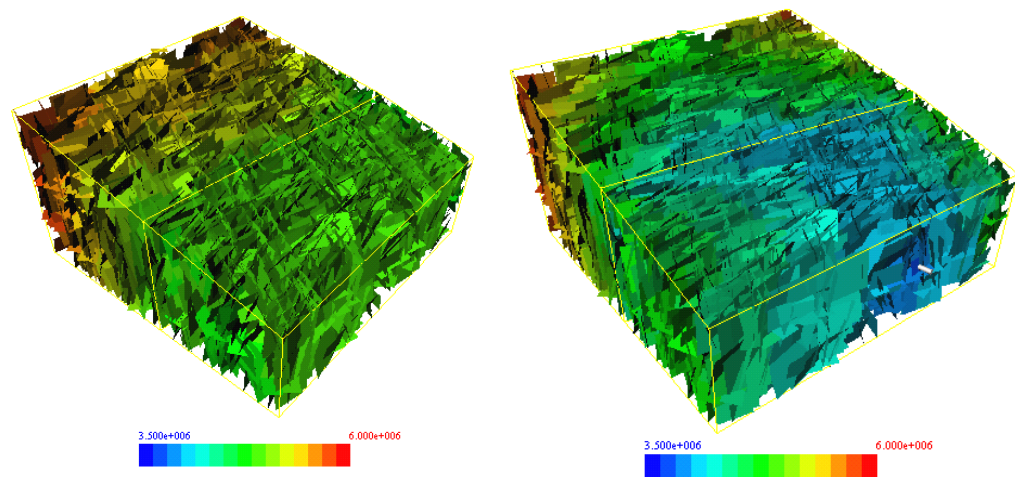


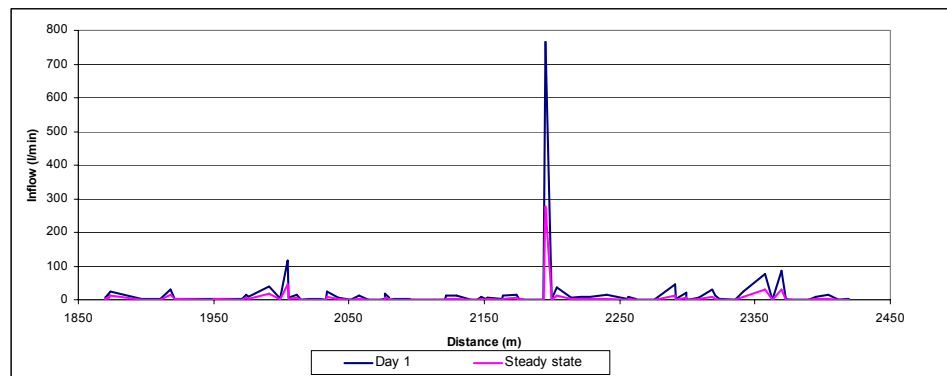
Fig. 3.9 Pressure solution and inflow data for Model 1 prior (A) and after tunnelling (B)

For Model 1 (Fig. 3.9C) there is only a small reduction in water inflow along zone K from day 1 until steady state is reached. This is probably because zone K is in direct contact with the boundary. In Model 2, boundary conditions BC-2 have also been prescribed, but the deterministic faults are not in contact with the boundaries. This results in a lower inflow into the tunnel for the steady state solution, indicating that the boundaries have less influence on the results.



A) Initial pressure conditions

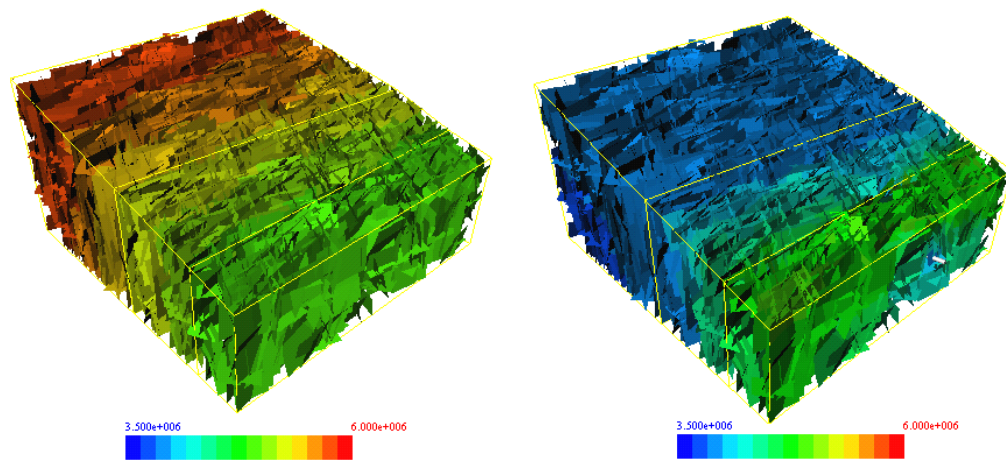
B) Pressure solution for steady state



C) Inflow in tunnel at day 1 and at steady state

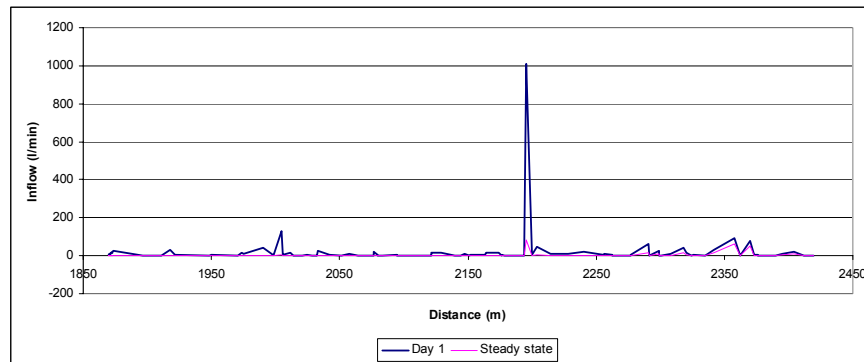
Fig. 3.10 Pressure solution and inflow data for Model 2 prior (A) and after tunnelling (B).

It is also obvious from Fig. 3.10B that the effect of the tunnel is more pronounced when the boundaries have less influence. Fig. 3.10B clearly shows a reduction in pressure (blue) over zone K that is striking N-S in the middle of the model.



A) Initial pressure conditions

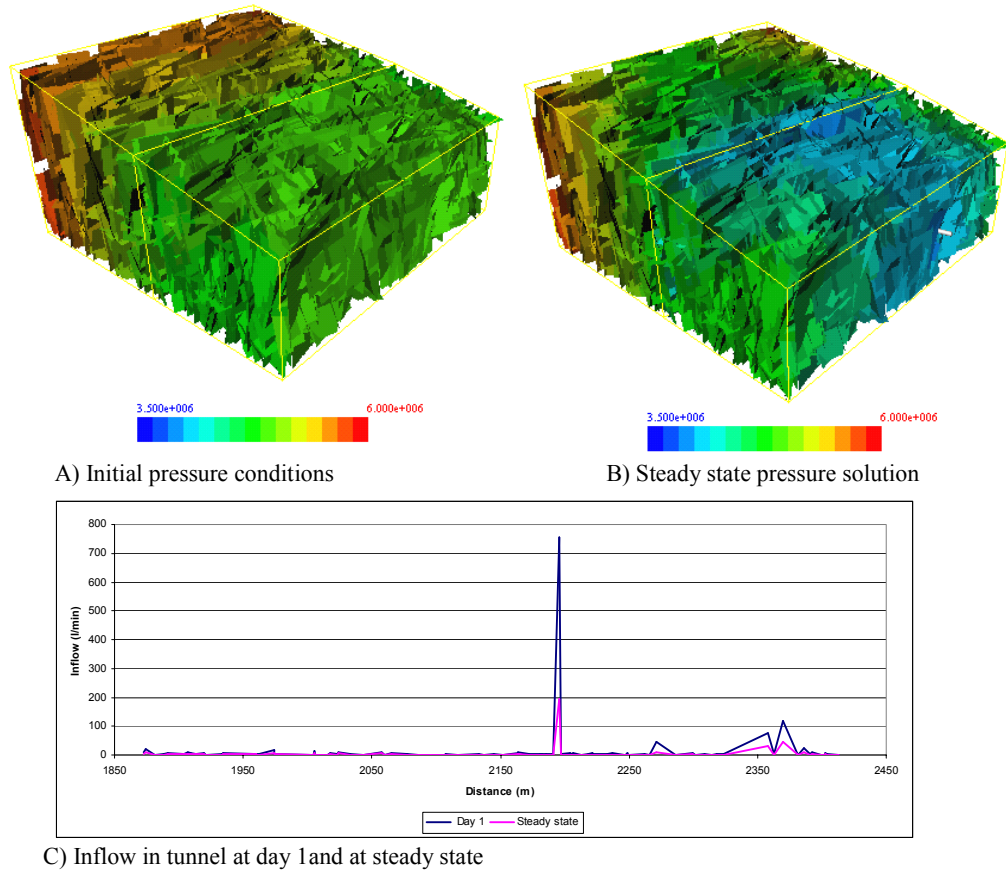
B) Steady state pressure solution



C) Inflow in tunnel at day 1 and at steady state

Fig. 3.11 Pressure solution and inflow data for Model 3 prior (A) and after tunnelling (B).

Model 4 (Fig. 3.12) is similar to Model 2, but the background fractures have been assigned a lower transmissivity value in the hornfels. This model shows a lower inflow from the hornfels into the tunnel both at day 1 (transient flow) and under steady state conditions (Fig. 3.12C, distance 1850-2200 m). In the syenite (distance 2200-2450m on the profile), a higher inflow is obtained for some fractures. The transition zone between the two different rock types shows the same leakage rate as in Model 2 (Fig 3.10C) under transient flow (day 1), but a lower one under steady state condition.



C) Inflow in tunnel at day 1 and at steady state
 Fig. 3.12 Pressure solution and inflow data for Model 4 prior (A) and after tunnelling (B).

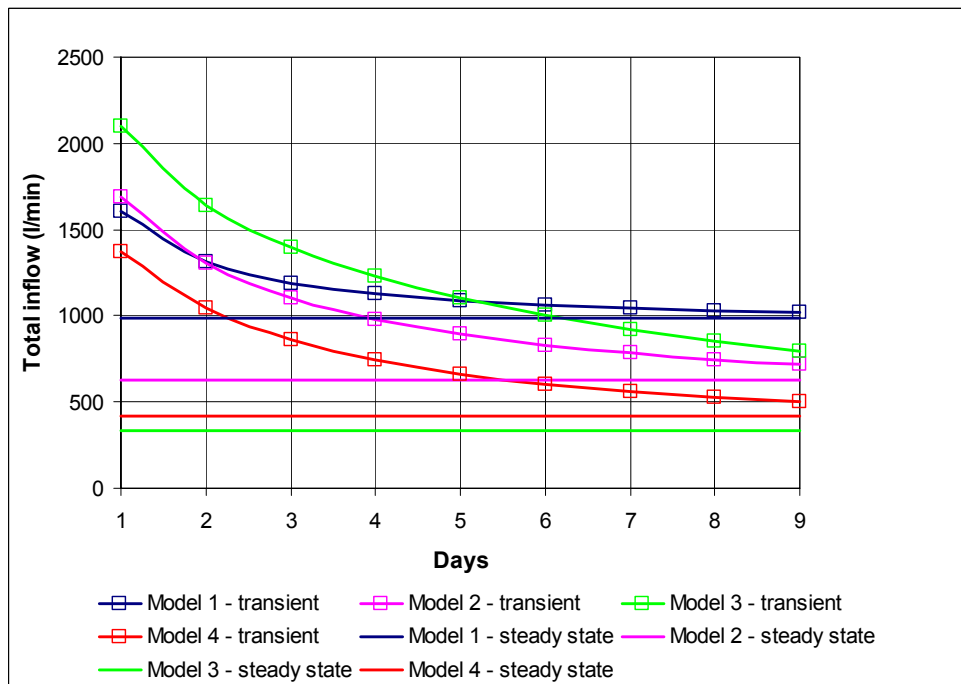


Fig. 3.13 Total inflow to the tunnel for Models 1, 2, 3 and 4.

Fig. 3.13 shows that for the first three days the inflow to the tunnel is the same for Models 1 and 2, whereas Model 3 (respect. Model 4) gives higher (respect. lower) inflow. After 9 days Models 1, 2 and 4 are close to steady state conditions, to the contrary of Model 3. A difference between Models 1 and 2 becomes only evident after the first three days, indicating the onset of boundary interaction.

3.4.5 Discussion of the results

The 3D groundwater flow model illustrates a possible leakage and groundwater drawdown scenario for a section of the Lunner tunnel. In Fig.3.14, the leakage rates predicted from Model 4 at day 1 and at steady state conditions have been cumulated over 100 meter tunnel section and are given in l/min per 100 meters. Leakage rates occurring after one day are probably comparable with leakage rates observed during tunnel excavation, whereas the leakage rates under steady state conditions are much reduced due to pore pressure reduction around the tunnel. Based on the input parameters, leakage rates in the order of 50-100 l/min per 100m tunnel are predicted in the hornfels. Higher leakage rates in the order of 80-250 l/min per 100m tunnel are predicted in the syenite section. In the weakness zone K at the transition between the two rock types, the leakage rate is high, in the order of 850 l/min per 100m tunnel.

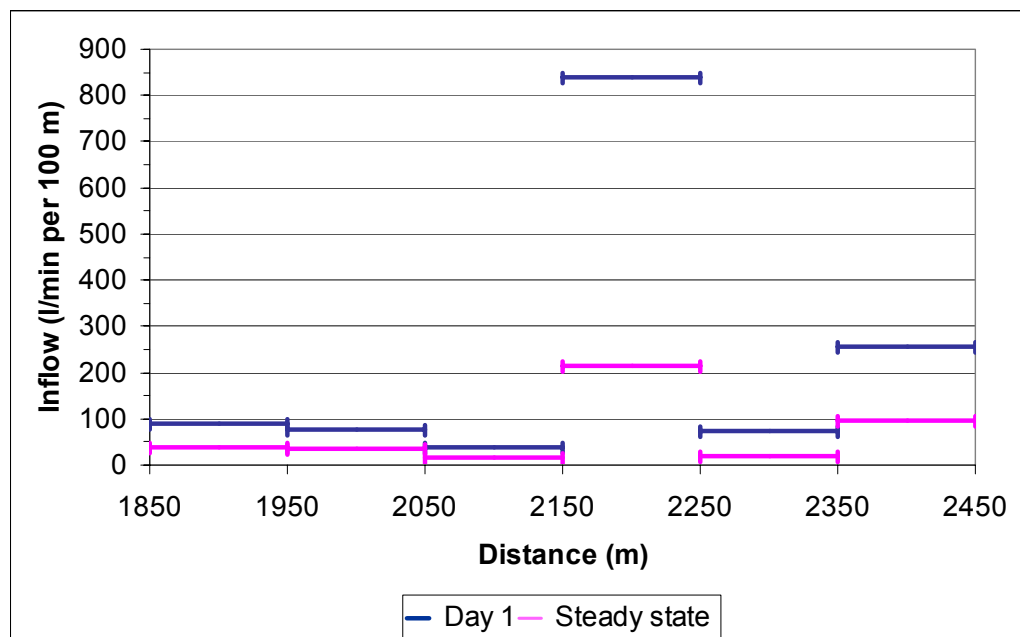


Fig. 3.14 Leakage rates for tunnel section (profile nr 1850 -2450) based on Model 4

Fig.3.15 shows the pressure distribution in Model 2 as calculated by Napsac under steady state conditions. Let us recall that Napsac works with the dynamic pressure, so that the pressure at tunnel level is roughly equal to $\rho g h_{\text{tunnel}} \approx 3.7$ MPa.

The pore pressure reduction caused by tunnel leakage tends to follow the structural heterogeneities in the model area. Low pore pressure areas can be seen around the tunnel and the weakness zone K. The pore pressure is also lower in the syenite than in the hornfels due to the declining topography towards the east.

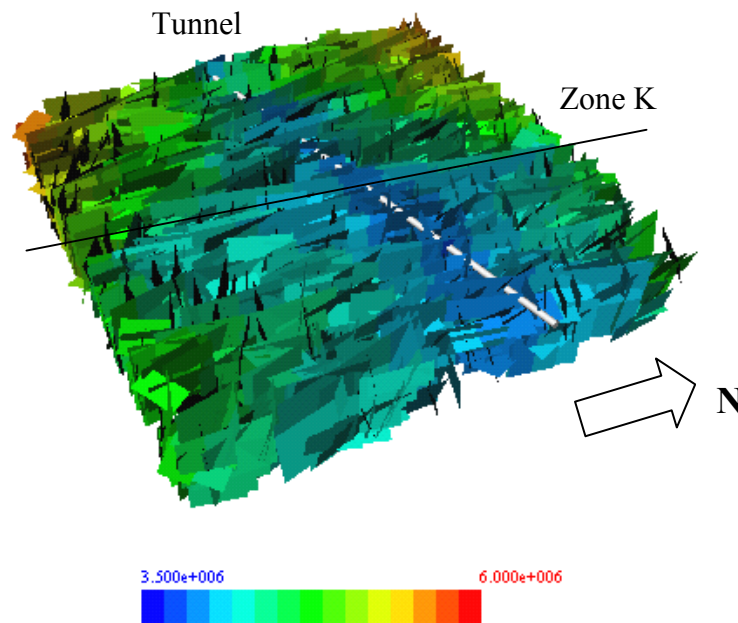


Fig. 3.15 Steady state pressure solution (in Pa) for Model 2 at tunnel level. The influence of the tunnel propagates along zone K, as depicted by a low- pressure contour.

The predicted groundwater drawdown from Model 4 is shown in Fig.3.16 for the central part of the modelled area. The contour plot is based on pore pressure data extracted from 15 fictitious observation wells in Model 4. The maximum drawdown is around 90 meters, and clearly correlates not only with the tunnel trace but also with the weakness zone K. The drawdown is higher on the eastern side of zone K, where the tunnel goes through the more permeable syenite. Note that the contour plot might be somehow biased by the relatively few number of observation wells. Lower drawdown on the northern side of the tunnel than on the southern side along the weakness zone K is probably due to a lack of measuring points close to zone K.

The results from the modelling show that without injection, the effect of tunnel excavation on the groundwater table is very important. A large drawdown is predicted, which means that the rock formations overlying directly the tunnel will be emptied for water. Note also that the leakage rates predicted are usually one to two orders of magnitude above the critical leakage rates estimated by Jordforsk (Kløve et al., 1999) that the environment could sustain (in the range 10 to 20 l/min per 100 m tunnel).

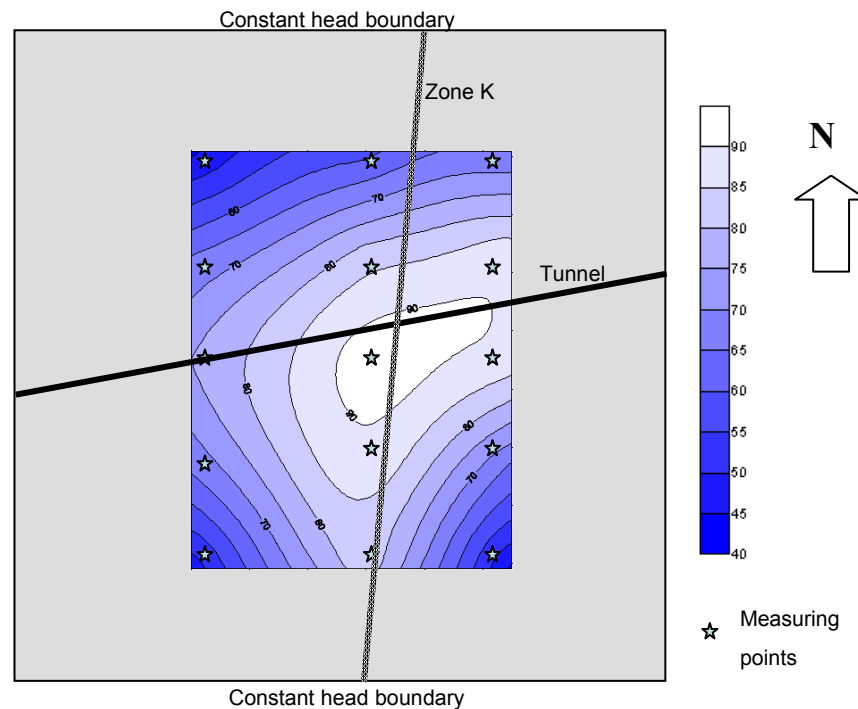


Fig. 3.16 Contour plot showing groundwater drawdown (in meter) for the central part of the model area (275m x 360m). The whole model area is shown with grey colour.

3.5 The effect of cement injection

3.5.1 Introduction

In this section, the effect of cement injection in the weakness zone is investigated. The process of cement injection is not taken into account in the model. Instead the injection interval is assigned a given transmissivity which is representative of “cemented conditions”. The transmissivities of the fractures intersecting the interval are then modified (“conditioned” in statistical terms) with the constraint that the original statistical distribution of transmissivity is preserved.

Due to the limitation in Napsac with respect to conditioning deterministic faults, the weakness zone K has been represented in the following as a 20m wide zone where the intensity of background fracturing is increased by a factor three. Other characteristics of the model used for the analysis (Model 5) are similar to Models 1-3.

The transmissivity of background fractures in the injection interval is modified as follows:

$$T_{ci} = \frac{T_c * T_i}{\sum T_i} \quad (3.4)$$

where T_c is the transmissivity of the injection interval, T_i and T_{ci} are respectively the unconditioned and conditioned transmissivities of a fracture within the interval.

Note that the technique cannot be used to assess the efficiency of the injection process, but the effect of reduced leakage on groundwater drawdown.

3.5.2 Result of cement injection along the whole tunnel

A series of tests have been carried out to see the effect of reduced fracture transmissivity on water inflow along the tunnel. It is assumed that cement injection has been carried out along the whole tunnel. Table 3.6 and Fig.3.17 show the relationship between the reduction of transmissivity achieved in a “cemented” fracture and the corresponding reduction in total inflow for the tunnel. In the figure, the reduction in inflow is also plotted against the equivalent reduction of fracture aperture. The trend between reduced flow and aperture is more or less linear. The water inflow along the tunnel is shown in Fig.3.18 for the different transmissivity reduction factors. For comparison, without injection, the total inflow into the tunnel is equal to circa 210 l/min per 100 m tunnel on average.

Table 3.6 Transmissivity reduction for “cemented” fractures and corresponding reduction in total tunnel inflow.

Transmissivity reduction in “cemented” fracture (%)	80	90	95	98	99	99.5
Tunnel inflow (l/min per 100 m)	117	84	57	31	19	11
Reduction in inflow due to injection (%)	45	60	73	85	91	95

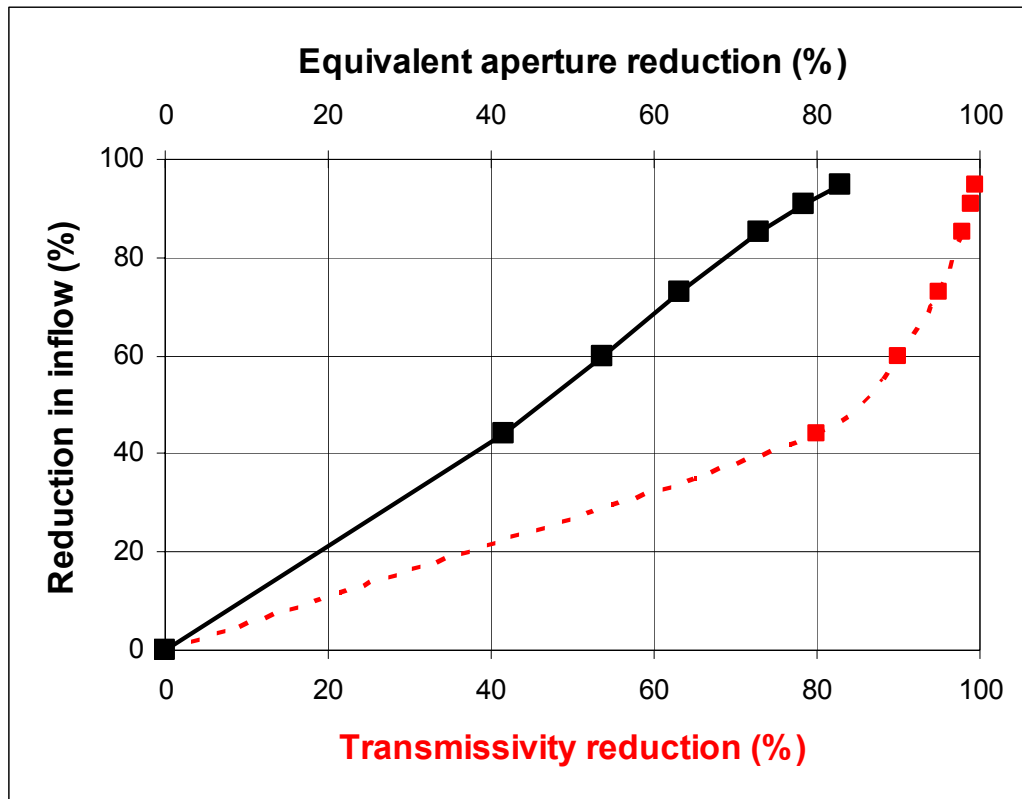


Fig. 3.17 Reduction in water inflow against reduction in transmissivity (in red dashed line) or equivalent fracture aperture (in black plain line).

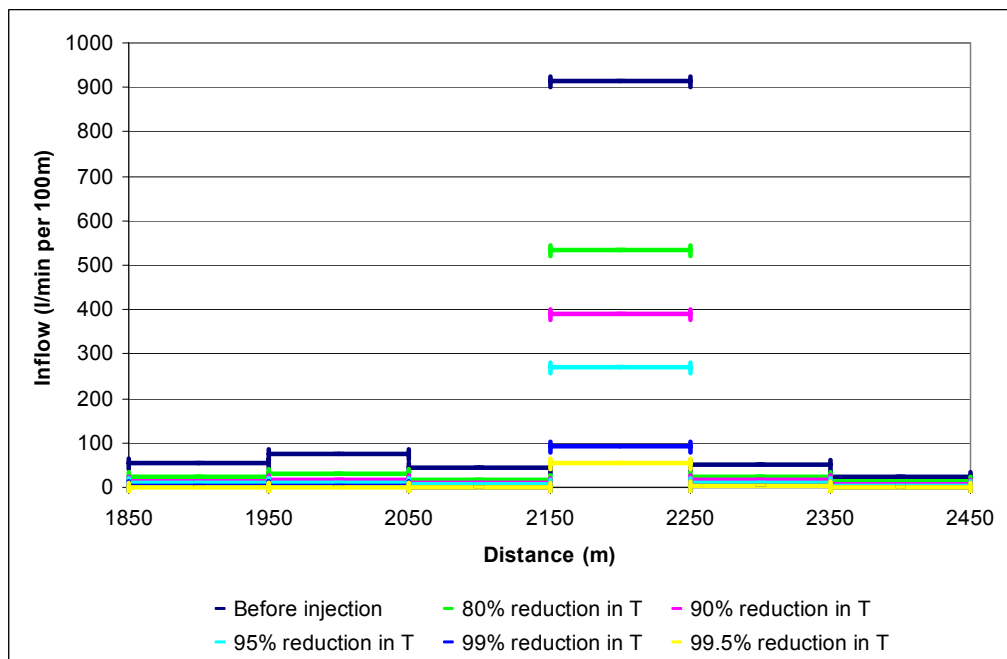


Fig. 3.18 Water inflow along the tunnel for various transmissivity (T) reductions of "cemented" fractures.

The pore pressure distribution and groundwater drawdown in the central part of the model area are shown in Fig. 3.19. Without injection, a groundwater drawdown of 90 m is observed directly above the tunnel trace, and propagates slightly into the rock formation along the weakness zone (Fig. 3.19A). If one assumes that the transmissivity of cemented fractures has been reduced by 95%, the total inflow into the tunnel is then reduced by 73%, as given in Table 3.6. The corresponding contour map of groundwater drawdown and pore pressure distribution is shown in Fig. 3.19B. In that case, a 25m groundwater drawdown is observed above the tunnel in the central part of the model. Finally if the transmissivity of cemented fractures has been reduced by 99.5%, a maximum drawdown of 4.5m is obtained, associated with a 95% reduction of the total tunnel inflow.

At the western side of the weakness zone K the contour plot indicates that the groundwater gradient is more controlled by the topography of the model area than the tunnel. Generally, there is a higher drawdown on the eastern side of the weakness zone where the overlying rock mass is thin.

3.5.3 Result of cement injection within an interval

In this section, only the portion of the tunnel crossing the weakness zone K has been subjected to cement injection. It is assumed that a transmissivity reduction of 99.5% has been achieved within the injection interval. The results are shown in Fig.3.20 in terms of water inflow along the tunnel. As seen from the figure, the reduction of water inflow in the weakness zone is associated with a slight increase of water inflow outside the injection interval on both sides of the weakness zone. The zone influenced by the increase in water inflow is roughly 75-100m long on both sides of the weakness zone, whereas the weakness zone being sealed is only 55m long. The total inflow into the tunnel has been reduced by 56% by injecting into the weakness zone (total inflow equal to 92 l/min per 100m tunnel after injection). This figure can be compared to a 90% reduction in transmissivity obtained with systematic injection over the whole tunnel length. This result indicates that massive injection campaigns in weakness zones may be more effective than a moderate injection campaign along the whole tunnel.

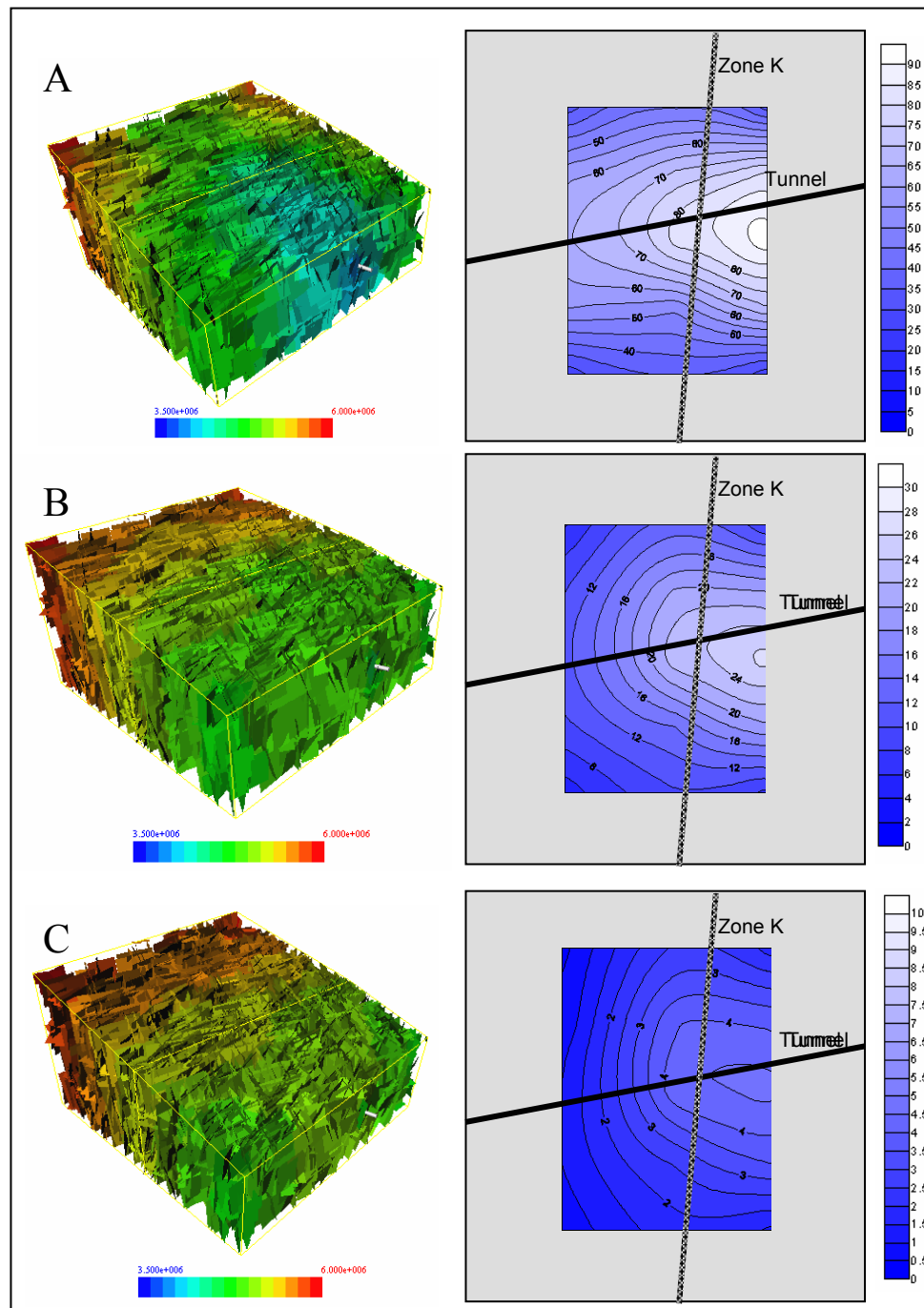


Fig. 3.19 Steady state pore pressure distribution (in Pa) for the 3D model and contour map (meter drawdown) for the corresponding groundwater drawdown. A) Without cement injection. B) Injection giving a 73% reduction in total inflow. C) Injection giving a 95% reduction in total inflow.

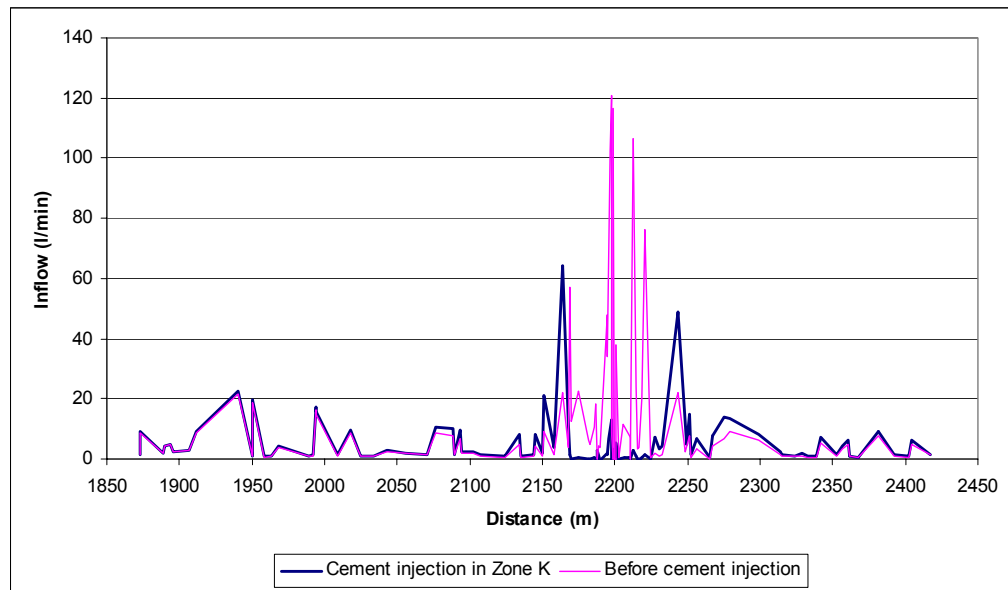


Fig. 3.20 Water inflow along the tunnel before and after cement injection of weakness zone K (distance 2170-2225m). The transmissivity of “cemented” fractures is assumed to be reduced by 99.5 %



4 CONCLUSIONS AND RECOMMENDATIONS FOR FUTURE WORK

4.1 Conclusions

As part of the project “Tunnels for the citizen”, sub-project B “Environmental concerns”, coordinated by the Norwegian Road Authority (“Statens vegvesen”), a discrete fracture network model was used to investigate the hydrogeological conditions before and after construction of the Lunner tunnel. In contrast to a continuous model where flow takes place in a porous material, the discrete fracture approach places a large emphasis on fractures and faults that dominate the flow system and contribute to the hydraulic heterogeneity of the rock mass. Many authors have shown that continuous models for fractured rocks cannot adequately represent locally the hydraulic interaction between an excavation (tunnel, underground repository...) and the surrounding rock mass due to the presence of fractures. Continuous models may nevertheless be used at a larger scale, when only average flow behaviour is of interest. At this scale computational limits impose also constraints on the use of discrete fracture network models.

The size of investigation was therefore reduced to an area of 550 m x 550 m comprising the transition zone from two rock types (hornfels and syenite) where potential problems were foreseen. Available data from site investigation performed by Statens vegvesen and NGU was used to build the model. First, large scale features which could be geologically mapped were represented deterministically. Smaller scale features which could only be characterised in a statistical sense from boreholes observation in terms of orientation, dip, length, density were used to stochastically generate discrete fracture networks through which water flows. Saturated transient and steady state calculations were performed to predict the amount of leakage into the tunnel during construction. Only linear groundwater flow was considered, with a constant recharge from precipitation. Due to the uncertainty related to crucial input parameters such as fracture length and fracture hydraulic properties, a parametric analysis was carried out to investigate the range of variation in the model predictions.

The results from the modelling give a three dimensional picture of the groundwater level after tunnel excavation. They outline the interrelation between tunnel and main conductive faults in the establishment of a lowered water table. Due to tunnel excavation, a rapid drawdown is established above the tunnel and propagates into the rock mass along conductive fault zones. Injection of the faulted zone contributes to a drastic reduction in leakage rates in the whole tunnel, although locally the water inflow increased on both sides of the injection interval through secondary fracture sets.

The work presented in this report contributed to:

- assess the capabilities of discrete fracture network models generally, and more specifically their application to modelling of groundwater flow around tunnels in fractured rock masses

- test the commercial software Napsac used for the purpose of the analyses
- carry out a blind prediction of the effect associated with tunnel excavation in a potentially sensitive area, based on data collected during pre-investigation work
- evaluate the results from discrete fracture modelling and the sensitivity to input parameters. Of particular interest were the correlations between tunnel leakage, pore pressure changes and groundwater drawdown, which could be used to define acceptance criteria for tunnel leakage based on the vulnerability of vegetation and water sources.

The following conclusions can be drawn with respect to the set-up of a hydrogeological model with discrete fracture networks:

- Discrete fracture networks must include major conductors (fracture zones, faults, rock boundaries) represented as deterministic features superposed on a background of stochastically generated features. It is important to be able to distinguish between the two types during the interpretation of field data
- Geologically observed networks do not necessarily coincide with hydrologically active networks, so that correlation between geological model and flow is not straightforward
- Basis input data concern the position, geometry and hydraulic properties of the deterministic features, as well as the number of stochastic fracture sets, and for each set statistics related to the fracture orientation, fracture distribution in space and the hydraulic properties of the fracture. The data must be representative for the area of investigation.
- The boundary conditions used in the numerical model have a considerable influence on the flow results especially for small models. Direct connection between deterministic conductive fault planes and boundaries gave in some cases unrealistic flow conditions.

The following capabilities were tested with the commercial code, Napsac used in the analyses:

- The hydraulic properties of the background fractures could be calibrated by reproducing Lugeon tests carried out in situ.
- The code could be used to perform sensitivity analyses and evaluate the effect of input parameters on the hydrogeological conditions prior and after tunnelling
- The modelling of an engineered feature such as a tunnel, gave very good results
- Cement injection in a section or the whole tunnel could be simulated by conditioning the distribution of fracture transmissivity to a given value.
- Statistical predictions of inflow / groundwater drawdown etc could be made with stochastic generation of fracture distribution.

- The code could be used to assess the time-dependency of leakage rates, and model transient flow as well as steady state.

The following conclusions can be drawn with respect to the modelling results obtained in the analyses:

- First class predictions of water inflow into the tunnel are not easy, as many parameters are uncertain, and difficult to estimate from field data. In particular few data is available on the transmissivity of large weakness zones, and much speculative work has to be done
- Water inflow along the tunnel is generally high due to the high transmissivity and good percolation of the background fracture network. This may partly be related to the fact that input data available is mainly from wells and boreholes aiming at weakness zones with high fracture density and open fractures. Little data is available at tunnel depth
- Pore pressure reduction along the tunnel and weakness zones resulted in a large groundwater drawdown. The presence of a weakness zone crossing the tunnel increased the influence zone around the tunnel
- Drawdown is highest in parts of the model with low rock mass cover
- Cement injection reduces the drawdown, although high transmissivity reductions must be achieved in the fractures in order to reduce drastically the leakage rates. Massive injection campaigns in weakness zones may be more effective than a moderate injection campaign over the whole tunnel.
- Injection in a weakness zone results in a slight increase in water inflow on the outside of the injection zone.

4.2 Recommendations for future work

Although promising, the results outline the need for further analyses in the area of:

- interaction with the overlying sediments. Groundwater in hard rocks is mostly stored in the overlying sediments, since the porosity of the hard rock is usually limited. Fractures act as drainage channels from the excavation to the overlying sediments. Large inflow problems can be expected in the areas having larger groundwater storage capacity and good connection between excavation and sediments. Therefore leakage prediction are not only regulated by the structure of the rock, but also by the nature and thickness of the overlying sediments. Better prediction of tunnel inflow can be achieved if the interrelated system sediments and bedrock is considered. As part of the interaction, a better modelling of precipitation should be performed by considering 1) the transient nature of the phenomenon, 2) the limited recharge capacity of the bedrock for net infiltration, 3) the existence of an unsaturated zone (vadose zone).



- The scope of investigation could be widened in order to make more generic conclusions and recommendations pertaining to the effect of tunnel leakage on groundwater flow, and the use of discrete fracture network models prior to tunnel construction. In particular, a comparison with a continuous approach should be performed to highlight the difference between methods and their respective benefits and disadvantages. Comparison should be made with leakage data from existing constructions.



5 REFERENCES

1. Aarseth E.S. Bourguine B. Castaing C. Chilès J.P. Christensen N.P. Eelse M. Fillion E. Genter A. Gillespie P.A. Håkansson E., Zinck Jørgensen K., Lindgaard H.F., Madsen L., Odling N.E. Olsen C. Reffstrup J. Trice R. Walsh J.J. Watterson J. (1997) "Interim guide to fracture interpretation and flow modelling in fractured reservoirs". EEC Report No EUR 17116EN.
2. Cacas M.C., Ledoux E., de Marsily G., Tillie B., Barbreau B., A. Durand, B. Feuga, P. Peuadecarf. Modeling fracture flow with a stochastic discrete fracture network: calibration and validation. 1, The flow model. Water Resources Res., 26 (3) 479-489 (1990)
3. Dershowitz W. (1993) Geometric conceptual models for fractured rock masses: implications for groundwater flow and rock deformation. Eurock'93, Ribeiro e Sousa & Grossmann (eds), Balkema, pp.71-81
4. Dreuzy J.R. Davy P. Bour O. Hydraulic properties of two-dimensional random fracture networks following a power law length distribution. Water Resources Research, Vol. 37, No.8, 2065-2078 (2001)
5. Elvebakk, E., Rønning, J.S., Braathen, A., Nordgulen, Ø. 2001. Tunnelprosjektet. Borhullslogging og strukturgeologiske studier Gualia, Lunner kommune. NGU Rapport 2001.117.
6. Hartley L.J. Napsac Release 4.1 Technical Summary document. AEA-D&R-0271. (1998)
7. Herbert A.W. Lanyon G.W. Gale J.E. Macloed R. Discrete fracture network modelling for phase 3 of the Stripa project using Napsac. Proceedings of the 4th international symposium on the NEA/OECD Stripa project, OECD, 1992
8. Iversen, E., 1998. Rv.35 Gualia-Slettmoen, Kjerneboring for tunnel under Langvann. Statens Vegvesen, rapport nr. E-218 A nr. 3.
9. Kirkeby, T. & Iversen, E., 1996. Rv.35 Gualia – Slettmoen, tunnel gjennom Tveitmarkstoppen. Geologiske undersøkelser for detaljplanen. Statens Vegvesen, oppdrag E-218A, rapport nr. 2.
10. Kløve B. Kværner J. Hydrogeologiske konsekvenser av vegtunnel Gualia-Bruvoll. Statusrapport 2001. Jordforsk Rapport nr 72/01.(2001)
11. Kløve B. Gaut A., Kværner J., 1999. Hydrologiske konsekvenser av vegtunnel Gualia - Bruvoll; Sårbarhet, vannbalanse og lekkasjekriterier. Jordforsk Rapport nr 9/99.
12. Miljø og Samfunnstjenlige Tunneler (2002). Oppsummering av utførte undersøkelser og prognose for innlekkasje ved Gualiatunnelen. Rapport nr 15, Statens vegvesen. Mai 2002.
13. NGI (1999). NGI Report No 543073-1 entitled "Forurensningstransport og permeabilitet i oppsprukket fjell. Sammenheng mellom oppsprekking i borhull og permeabilitet"



14. Niemi A. Kontio K. Kuusela-Lahtinen A. Hydraulic characterization and upscaling of fracture networks based on multiple-scale well test data. *Water Resources Research*, Vol. 36 No. 12, pages 3481-3497
15. Odling N.E: Derivation of a fracture aperture model and hierarchical flow modelling applied to the fracture system in Hornelen, Western Norway. In *Interim Guide to fracture interpretation and flow modelling in fractured reservoirs*. EUR 17116 EN (1997)
16. Priest S.D. *Discontinuity analysis for rock engineering*. Chapman et Hall (1993)
17. Snilsberg P. Kløve B. Borebrønner Grua / Lunnerhøgda. *Jordforsk Notat* datert 6 april 2001 (2001)
18. Tsang Y. Usage of equivalent apertures for rock fractures as derived from hydraulic and tracer tests. *Water Resour. Res.* 28 (5), 1451-1455 (1992)
19. Uchida M. Doe T. Dershowitz W. Thomas A. Wallman P. Sawada A. Discrete fracture modelling of the Äspö LPT-2 large scale pumping and tracer test. *SKB Int. Co-op Rep. 94-09*, Swed. Nucl. Power and Waste Manage. Co., Stockholm (1994)
20. Wilcock P. The Napsac fracture network code. In *Coupled Thermo-Hydro-Mechanical Processes of Fractured Media*, 529-538 O. Stephansson, L. Jing and C.-F. Tsang (eds) (1996)

Kontroll- og referanseside/ Review and reference page



Oppdragsgiver/Client Prosjektet Miljø- og Samfunnstjenelige tunneler	Dokument nr/Document No. 20001042-2
Kontraksreferanse/ Contract reference Letter dated 2/3/2001	Dato/Date 4 March 2003
Dokumenttittel/Document title Prediction of leakage into Gualia tunnel based on discrete fracture flow models Prosjektleder/Project Manager Vidar Kveldsvik Utarbeidet av/Prepared by Fabrice Cuisiat & Elin Skurtveit	Distribusjon/Distribution <input type="checkbox"/> Fri/Unlimited <input checked="" type="checkbox"/> Begrenset/Limited <input type="checkbox"/> Ingen/None
Emneord/Keywords Tunnel , leakage, inflow, groundwater, discrete fracture network modelling	
Land, fylke/Country, County Akershus Kommune/Municipality Lunner Sted/Location Kartblad/Map 815I UTM-koordinater/UTM-coordinates 32V 945 828	Havområde/Offshore area Felt navn/Field name Sted/Location Felt, blokknr./Field, Block No.

Kvalitetssikring i henhold til/Quality assurance according to NS-EN ISO9001							
Kon- trollert av/ Reviewed by	Kontrolltype/ Type of review	Dokument/Document		Revisjon 1/Revision 1		Revisjon 2/Revision 2	
		Kontrollert/Reviewed		Kontrollert/Reviewed		Kontrollert/Reviewed	
		Dato/Date	Sign.	Dato/Date	Sign.	Dato/Date	Sign.
VK	Helhetsvurdering/ General Evaluation *	3 april '03	UK				
	Språk/Style						
	Teknisk/Technical - Skjønn/Intelligence - Total/Extensive - Tverrfaglig/ Interdisciplinary						
	Utforming/Layout						
VK	Slutt/Final	3 april '03	UK				
JS	Kopiering/Copy quality						
* Gjennomlesning av hele rapporten og skjønnsmessig vurdering av innhold og presentasjonsform/ On the basis of an overall evaluation of the report, its technical content and form of presentation							
Dokument godkjent for utsendelse/ Document approved for release		Dato/Date 3 april 2003		Sign. Vidar Kveldsvik			